Deletion of the Na-K-2Cl cotransporter NKCC1 results in a more severe epileptic phenotype in the intrahippocampal kainate mouse model of temporal lobe epilepsy

Philip Hampel [a,d,1], Marie Johne [a,b,1], Björn Gailus [a,b,1], Alexandra Vogel [a], Alina Schidlitzki [a], Birthe Gericke [a,b], Kathrin Töllner [a], Wiebke Theilmann [a], Christopher Käufer [a], Kerstin Römermann [a], Kai Kaila [c], Wolfgang Löscher [a,b,*]

[a] *Dept. of Pharmacology, Toxicology, and Pharmacy, University of Veterinary Medicine, Hannover, Germany*
[b] *Center for Systems Neuroscience, Hannover, Germany*
[c] *Molecular and Integrative Biosciences and Neuroscience Center (HiLIFE), University of Helsinki, Finland*
[d] *Neurona Therapeutics, San Francisco, CA, USA*

ARTICLE INFO

ABSTRACT

Increased neuronal expression of the Na-K-2Cl cotransporter NKCC1 has been implicated in the generation of seizures and epilepsy. However, conclusions from studies on the NKCC1-specific inhibitor, bumetanide, are equivocal, which is a consequence of the multiple potential cellular targets and poor brain penetration of this drug. Here, we used *Nkcc1* knockout (KO) and wildtype (WT) littermate control mice to study the ictogenic and epileptogenic effects of intrahippocampal injection of kainate. Kainate (0.23 μg in 50 nl) induced limbic status epilepticus (SE) in both KO and WT mice with similar incidence, latency to SE onset, and SE duration, but the number of intermittent generalized convulsive seizures during SE was significantly higher in *Nkcc1* KO mice, indicating increased SE severity. Following SE, spontaneous recurrent seizures (SRS) were recorded by continuous (24/7) video/EEG monitoring at 0-1, 4-5, and 12-13 weeks after kainate, using depth electrodes in the ipsilateral hippocampus. Latency to onset of electrographic SRS and the incidence of electrographic SRS were similar in WT and KO mice. However, the frequency of electrographic seizures was lower whereas the frequency of electroclinical seizures was higher in *Nkcc1* KO mice, indicating a facilitated progression from electrographic to electroclinical seizures during chronic epilepsy, and a more severe epileptic phenotype, in the absence of NKCC1. The present findings suggest that NKCC1 is dispensable for the induction, progression and manifestation of epilepsy, and they do not support the widely held notion that inhibition of NKCC1 in the brain is a useful strategy for preventing or modifying epilepsy.

1. Introduction

The Na-K-2Cl cotransporter NKCC1 (encoded by the *Slc12a2* gene) mediates active Cl⁻ uptake in a large variety of cell types within and outside the brain (Russell, 2000; Markadieu and Delpire, 2014). In the brain, NKCC1 is expressed in neurons as well as astroglia and oligodendrocytes (Wilson and Mongin, 2019; Virtanen et al., 2020). During development and disease of central neurons, NKCC1 acts together with the neuron-specific chloride extruder KCC2 as a major player in setting the reversal potential and driving force of the chloride currents mediated by GABA$_A$ receptors (Kaila et al., 2014a, 2014b). Because of the role of NKCC1 and KCC2 in controlling the efficacy of neuronal inhibition, many studies have addressed the potential impact of these ion transporters in the acute generation of seizures (ictogenesis) and in

---

epileptogenesis (reviewed in Kahle et al., 2008; Blaesse et al., 2009; Ben-Ari et al., 2012; Miles et al., 2012; Löscher et al., 2013; Kaila et al., 2014a, 2014b; Auer et al., 2020; Liu et al., 2020). For instance, in hippocampal brain slices from adult patients with temporal lobe epilepsy (TLE), downregulation of KCC2 and upregulation of NKCC1 leads to depolarizing GABA$_A$ receptor responses in a subpopulation of subicular principal neurons (Cohen et al., 2002; Huberfeld et al., 2007; Munoz et al., 2007). We and others have reported similar findings in the kindling and pilocarpine rat models of TLE (Rivera et al., 2002; Okabe et al., 2003; Pathak et al., 2007; Li et al., 2008; Brandt et al., 2010; Barmashenko et al., 2011; Kourdougli et al., 2017).

The potential role of upregulated neuronal NKCC1 in epilepsy has led to the suggestion that the NKCC1 inhibitor bumetanide may exert anticonvulsant and antiepileptogenic effects (Kahle and Staley, 2008; Kahle et al., 2008; Ben-Ari et al., 2012; Ben-Ari, 2017; Kharod et al., 2019; Auer et al., 2020; Liu et al., 2020). However, both preclinical and clinical data on bumetanide are controversial, which may be due to the fact that this loop diuretic only poorly penetrates into the neonatal or adult brain and consequently, at clinically used doses (0.05-0.3 mg/kg in pediatric patients, 0.5-2 mg in adult patients), does not reach brain levels that are sufficient to inhibit neuronal NKCC1 (Brandt et al., 2010; Löscher et al., 2013; Cleary et al., 2013; Puskarjov et al., 2014; Töllner et al., 2014; Brandt et al., 2018; Hampel et al., 2021).

Surprisingly, despite the availability of *Slc12a2* (or *Nkcc1*) knockout (KO) mice, they have only rarely been used to study the role of NKCC1 in ictogenesis and epileptogenesis. Constitutive *Nkcc1* KO mice are deaf and (as a result of their inner ear defects) exhibit unusual head postures, circling behavior, rapid spinning and difficulty in maintaining balance (Markadieu and Delpire, 2014). Zhu et al. (2008) reported that absence of NKCC1 in neonatal CA3 pyramidal neurons, through genetic manipulation or through bumetanide inhibition, results in a significant *increase* in cell excitability. Furthermore, the proconvulsant agent 4-aminopyridine induced seizure-like events in NKCC1-null mice but not in wild-type (WT) mice (Zhu et al., 2008). Sipilä et al. (2009) found that hippocampal slices from *Nkcc1*$^{-/-}$ neonates of the mouse line used in the present study (Flagella et al., 1999) generate endogenous network events similar to giant depolarizing potential (GDPs), most likely based on homeostatic upregulation of intrinsic neuronal excitability as a response to the lack of NKCC1-mediated GABAergic excitation; furthermore, glutamatergic network activity was enhanced in the *Nkcc1*$^{-/-}$ hippocampus.

Systemic treatment with clinically relevant doses of bumetanide (0.1-0.2 mg/kg) has been reported to exert anticonvulsant and antiepileptogenic effects in neonatal rodent models (Dzhala et al., 2005; Koyama et al., 2012; Cleary et al., 2013), but other studies have refuted this (Kang et al., 2015; Johne et al., 2021; see also Vanhatalo et al., 2009), and even high systemic doses of bumetanide did not alter epileptogenesis in the pilocarpine model in adult rats (Brandt et al., 2010). Interestingly, bumetanide (0.2 or 2 mg/kg) was reported to reduce kainate-induced seizure progression and the development of pharmacoresistant status epilepticus (SE) in adult mice (Sivakumaran and Maguire, 2016).

To our knowledge, the present study is the first that uses *Nkcc1* KO mice to determine the effect of genetic NKCC1 deletion on epileptogenesis. For this purpose, we used the intrahippocampal kainate mouse model of mesial TLE, in which increased NKCC1 expression has been reported to occur four weeks after SE in the ipsilateral hippocampus (Stamboulian-Platel et al., 2016). Focal, unilateral injection of kainate into the hippocampus mimics the onset and progression of human mesial TLE more closely than models with systemic administration of convulsants such as kainate or pilocarpine, since it causes unilateral cell death similar to the hippocampal sclerosis associated with clinical TLE (Guillemain et al., 2012; Duveau and Roucard, 2017).

In the present study, upregulation of NKCC1 expression was observed already at 24 h after SE in WT mice. Strikingly, the *Nkcc1* KO mice exhibited a more severe SE than WT littermates, and the

progression of spontaneous electrographic to electroclinical seizures was facilitated, resulting in a more severe epileptic phenotype. These data contradict the view that either the presence or upregulation of neuronal NKCC1 are critically involved in the development of epilepsy and that, as a consequence, pharmacological inhibition of NKCC1 may prevent or attenuate epileptogenesis after brain insults.

2. Materials and methods

2.1. Animals

The mouse strain with a disruption of *Slc12a2* coding for NKCC1 (Flagella et al., 1999) was obtained from The Jackson Laboratory and backcrossed into C57BL/6. WT, heterozygous, and homozygous *Nkcc1* KO mice of both sexes were generated from heterozygous matings. Genotyping was performed by using ear samples (ear punches) as described previously (Flagella et al., 1999). The germ-line homozygous *Nkcc1* KO animals have no expression of NKCC1 in any cells and tissues.

In the present study, male and female homozygous *Nkcc1*$^{-/-}$ mice and WT littermates were used. Animals were housed at 22-24 °C, humidity 30-50%, lights on from 6:00 am to 6:00 pm. Food (Altromin 1324 standard diet; Altromin, Lage, Germany) and water were freely available. Experiments were performed according to the EU council directive 2010/63/EU and the German Law on Animal Protection ("Tierschutzgesetz"). Ethical approval for the study was granted by an ethical committee (according to §15 of the Tierschutzgesetz) and the government agency (Lower Saxony State Office for Consumer Protection and Food Safety; LAVES) responsible for approval of animal experiments in Lower Saxony (reference number for this project: 15/1825). All efforts were made to minimize both the suffering and the number of animals. All animal experiments in this study are reported in accordance with the ARRIVE guidelines (Kilkenny et al., 2010). Furthermore, in line with guiding principles for biomedicine (Clayton and Collins, 2014), we accounted for sex as a biological variable in the present preclinical experiments.

2.2. Intrahippocampal kainate model

In this model, SE is induced by unilateral injection of kainate into the dorsal hippocampus (Suzuki et al., 1995; Bouilleret et al., 1999). Mice (age 10-15 weeks) were anesthetized with chloral hydrate (500 mg/kg i. p.), and kainate monohydrate (0.23 μg in 50 nl saline; i.e., 0.92 nM; Sigma-Aldrich, Steinheim, Germany), was stereotaxically injected into the right CA1 of the dorsal hippocampus over 60 s with a 0.5 μl microsyringe. In preliminary experiments on the mice used here, stereotaxic coordinates (according to Paxinos and Franklin, 2012) were determined by histological verification of the injection site in CA1. These coordinates were then used for the experiments on the WT and *Nkcc1* KO mice: ♀AP: −1.90 mm, L: −1.40 mm, V: −1.70 mm, ♂ AP: −1.90 mm, L: −1.60 mm, V: −2.0 mm. After injection of kainate, the needle was maintained *in situ* for additional 2 min to limit reflux along the injection track. For EEG recordings, the animals were immediately implanted with bipolar electrodes aimed at the site of kainate injection in the ipsilateral CA1, using the same coordinates as for kainate injection (see Gröticke et al., 2008). During all surgical procedures and for about 1 h thereafter mice were kept on a warming pad to avoid hypothermia.

The dose of kainate used in the present experiments (0.92 nM) was based on preliminary dose-effect experiments in male C57BL/6 WT mice, in which incidence of SE, mortality, and spontaneous recurrent seizures (SRS) were compared in groups of animals injected with either 0.92, 1.25, or 1.5 nM in the hippocampus. Incidence of SE and SRS was the same in all groups, but mortality was lowest in the 0.92 nM group.

In the present experiments with intrahippocampal injection of 0.92 nM kainate, WT littermates were always injected together with homozygous KO mice, using the same batch of kainate. Thus, there was no systematic difference in kainate injection between WT and KO mice.

In addition to the kainate-treated mice, additional age-matched WT mice (11 male, 11 female) were prepared as sham controls. These mice were treated in the same way as the kainate mice except that they received intrahippocampal injection of 50 nl saline instead of kainate.

Some experiments were also performed with pilocarpine, using a ramping-up i.p. dosing protocol of pilocarpine as described previously (Müller et al., 2009). All $Nkcc1^{-/-}$ and littermate controls died before developing SE in individual convulsive (tonic-clonic) seizures, due to respiratory arrest. High mortality in the pilocarpine model has been described previously for C57BL/6 mice (Borges et al., 2003; Müller et al., 2009); as a consequence, systemic administration of pilocarpine could not be used to study epileptogenesis in the mice used for the present study.

2.3. Video/EEG recording

After surgery, video-EEG monitoring was used to verify the limbic, predominantly nonconvulsive SE induced by kainate. Furthermore, as shown in Fig. 1, continuous (24/7) video-EEG monitoring over one week after kainate was used to determine the latent period, which, in previous experiments, ranged from 0 to 7 days (mean 2.1 days) in male C57BL/6 mice (Schidlitzki et al., 2020), whereas no clear latent period could be determined in female C57BL/6 mice (Twele et al., 2016a). Starting 4 weeks after SE, i.e., at a time at which the majority of kainate-injected mice exhibit SRS (Twele et al., 2016a, 2016b; Schidlitzki et al., 2020), continuous video-EEG monitoring over one week was used to compare the occurrence of seizures or other EEG abnormalities in kainate-injected WT vs. KO mice (Fig. 1). Video-EEG recording for one week was repeated after 12 weeks following kainate to determine if the progression of epilepsy was different between genotypes.

For EEG-recording, mice were connected via a flexible cable to a system consisting of one-channel amplifiers (ADInstruments Ltd., Sydney, Australia) and analog-digital converters (PowerLab 8/30 ML870, ADInstruments). The data were recorded and analyzed with LabChart 8 for Windows software (ADInstruments), sampling rate 200 Hz, time constant 0.1 s, low pass filter of 60 Hz, and a 50 Hz notch filter. The EEG-recording was directly linked to simultaneous digital video recording using one high-resolution infrared camera for up to eight mice (NYCTO Vision, CaS Business Services, Wunstorf, Germany). For video/EEG monitoring, mice were housed singly in clear plexiglass cages (one per cage). For monitoring during the dark phase, infrared LEDs were mounted above the cages.

2.4. Analysis of video-EEG activity during SE, latent period and the chronic epileptic state

Latency to SE onset, SE duration and severity were visually analyzed in the video-EEGs recorded from each mouse. During the latent period after SE, the EEGs recorded over 7 days after kainate were visually examined for onset of spontaneous electrographic seizure activity. Furthermore, electrographic and electroclinical seizures occurring in the chronic epileptic phase of mice with intrahippocampal kainate injection were analyzed visually.

Mice develop four types of epileptic SRS in this model, i.e., two types of electrographic (or nonconvulsive) seizures and two types of electroclinical (convulsive) seizures as described in the following. The most frequent SRS in this model are the two types of electrographic seizures in the the ipsilateral hippocampus without any obvious motor correlates (Twele et al., 2016a, 2016b). Based on the findings by Riban et al. (2002), we recently characterized these electrographic seizures for different mouse strains (Twele et al., 2016a, 2016b; Schidlitzki et al., 2020) and differentiated between high-voltage sharp waves (HVSWs) and hippocampal paroxysmal discharges (HPDs) as summarized in Table 1:

1. HVSWs (see also Fig. 2E-H and movie S1) are characterized by high amplitude sharp waves ≥3 times the EEG baseline with a frequency of at least 2 Hz (spikes per second), a duration of at least five seconds, and an inter-event interval of at least three seconds. The inter-event interval is characterized by the occurrence of either no epileptic EEG activity, isolated spikes, or spike trains with an amplitude of less than three times the baseline. HVSWs can show evolution in frequency or pattern, but can also appear uniform.

2. HPDs (Fig. 2I-L and movie S1) are often longer (over 20 s) than typical HVSWs and always show evolution in morphology and frequency. HPDs typically start with large-amplitude HVSWs, followed by a train of lower-amplitude spikes (≥ 2 times the baseline) with at least five seconds of increased frequency (≥ 5 Hz). As described previously (Twele et al., 2016b), based on duration, two types of HPDs occur: short HPDs (5-20 s) and, more often, long HPDs (>20 s). In the present study, both types were grouped together. Like HVSWs, HPDs also have an inter-event interval of at least three seconds, in which either no epileptic EEG activity, isolated spikes, or spike trains with an amplitude of less than two times baseline are observed (considered as interictal activity).

For comparison of the frequency of HVSWs and HPDs in WT and KO mice, electrographic seizures were counted manually in the EEG during
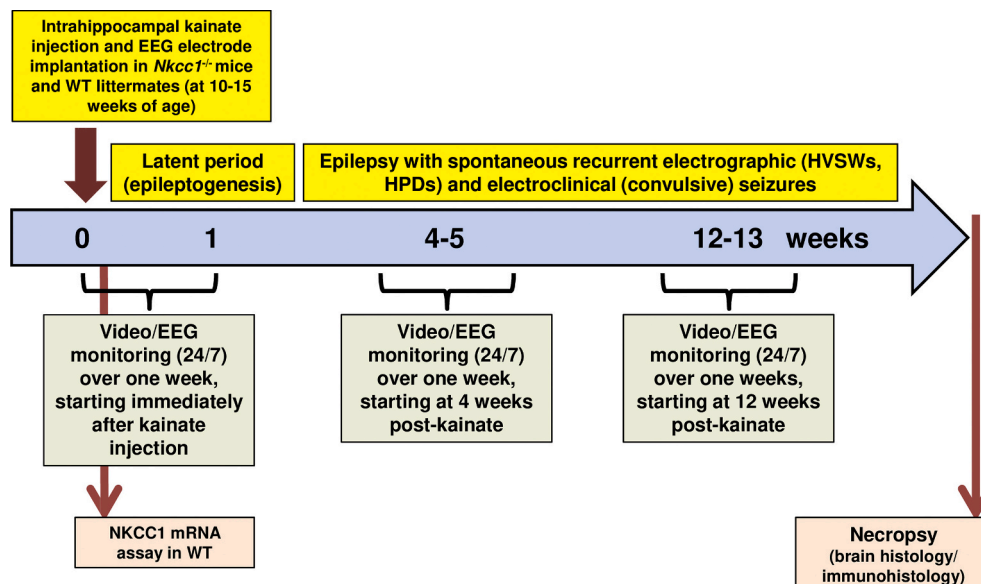

Fig. 1. Schematic presentation of the experimental protocol used for the present experiments.

Table 1

Comparison of the EEG characteristics of the three main types of seizures observed in the intrahippocampal kainate mouse model. These characteristics were defined previously in different mouse strains (Twele et al., 2016a, 2016b) and verified in the mice used for the present experiments. Seizure frequency (mean and range) refers to video/EEG recording in wildtype mice at 4-5 weeks after kainate. Fig. 2 gives representative examples of the different seizure types.

Parameter	Type of seizure		Electroclinical (convulsive)
	Electrographic (nonconvulsive or subclinical)		
	HVSW	HPD	
EEG alterations recorded from	Ipsilateral hippocampus (HVSWs are usually unilateral, but may also occur bilaterally)	Ipsilateral hippocampus (HPDs only occur in the immediate vicinity of the kainate focus)	Ipsilateral hippocampus (but occur in other brain regions)
Morphology	Sharp waves (often monomorphic)	Spikes and polyspikes (polymorphic)	Fast activity at onset, followed by irregular spiking; and periodic bursting that develops with time during the seizure (polymorphic)
Intra-event evolution	Often not	Yes	Yes
Spike frequency	≥2 Hz	≥5 s with ≥5 Hz, <3 s interruption with <5 Hz	≥2 Hz, typically ≥3 Hz
Amplitude	≥3 times baseline	Based on evolution ≥2-3 times baseline	Based on evolution ≥2-3 times baseline
Duration[a]	≥5 s	5- >20 sec[b]	≥10 s
Frequency	14.6/h (0-33/h)	3.5/h (0-18/h)	4.9/week (0-25)
Flattening of EEG after the seizure (post-ictal depression)	No	No	Yes
Inter-event interval	≥3 s	≥3 s	≥3 s
Behavioral alterations during paroxysmal EEG alterations	Not clearly visible in video recordings	Not clearly visible in video recordings[c]	Yes (focal and/or generalized convulsive seizures)
Comments	HVSWs can show evolution in frequency or pattern but often are rather regular.	Usually starts with HVSW-like activity; rate shows evolution with ≥5 Hz for ≥5 s.	Fulfill all arbitrary criteria of electroclinical seizures.

[a] In arbitrary definition of seizures, a duration of at least 10 s is often applied operationally, but there is no official minimum time to define a seizure (Fisher et al., 2014). Instead, it is frequently assumed that epileptiform discharges that last longer than 2–3 s can be considered as ictal.

[b] Based on duration, two types of HPDs: 5-20 s = short HPD, >20 s = long HPD.

[c] Behavioral arrest with head nodding or stereotyped behavior, such as exploration or grooming, were observed concomitantly with HPDs in several studies (Riban et al., 2002; Duveau and Roucard, 2017), but this is difficult to differentiate from normal activity during continuous video/EEG monitoring.

the two one-week video/EEG monitoring periods at 4 and 12 weeks post-SE. In each recording period, four 30-min periods (at 12:00, 6:00, and 11:00 pm of day 1 and 6:00 am of day 2) of continuous (24/7) EEG monitoring were selected and analyzed for calculation of the average number of electrographic seizures occurring per hour.

In addition to highly frequent electrographic seizures, mice develop less frequent focal and generalized electroclinical (convulsive) seizures (Twele et al., 2016b), which occur several times per week (Table 1).

Focal and generalized convulsive electroclinical seizures are characterized by a high spike frequency and amplitude, and a typical postictal depression of the EEG baseline (Fig. 2M,N and movie S1). For comparison of the frequency of electroclinical seizures in WT and KO mice, seizures were counted manually in the video/EEG recordings of the seven days of continuous (24/7) recordings at 4 and 12 weeks post-SE. Based on the video recordings, the electroclinical seizures were rated for severity using the following modified scale by Racine (1972): stage 1, behavioral arrest with minor facial clonus (stereotypical sniffing, tremor of tactile hair); stage 2, severe facial clonus (head nodding, mouth or facial movements); stage 3, unilateral forelimb clonus; stage 4, bilateral forelimb clonus with rearing; stage 5, generalized tonic-clonic seizure with loss of righting reflexes. Stage 1-2 seizures were considered as focal and stage 3-5 seizures as generalized convulsive seizures. Furthermore, the average severity and duration of electroclinical seizures was determined and compared between the two groups.

Some animals lost their electrode assemblies during the 3 months of the trial (see section 3). Thus, the videos were used to quantify electroclinical seizures in such mice. Therefore, the number of mice used for final analysis of electrographic and (electro)clinical seizures differs (see section 3). Here, it is relevant to note that we did not observe any electroclinical uncoupling in any individual during the present study, which justifies using the term "electroclinical seizure" in the small group of animals where the EEG recording was lost and convulsive seizures were seen.

2.5. Histology

For histological analysis, mice were deeply anesthetized with chloral hydrate (720 mg/kg i.p. in 10 ml) after the last video/EEG recording (13-14 weeks after intrahippocampal kainate injection; see Fig. 1) and transcardially perfused with 0.01 M phosphate-buffered saline followed by 4% paraformaldehyde. The brains were removed after one hour, postfixed in 10% sucrose solution (with 4% paraformaldehyde) for 24 h, and then transferred to 30% sucrose solution (saline). One mg/ml of thymol was added to the sucrose solution if the brains were stored for a longer period of time. As previously described (Bröer et al., 2016), four series of coronal brain sections (40 μm) were prepared using a cryomicrotome and subsequently stained with cresyl violet (containing thionin). Sham-treated mice were used as controls. The correct localization of the kainate injection and EEG electrode in the hippocampus was verified in each mouse.
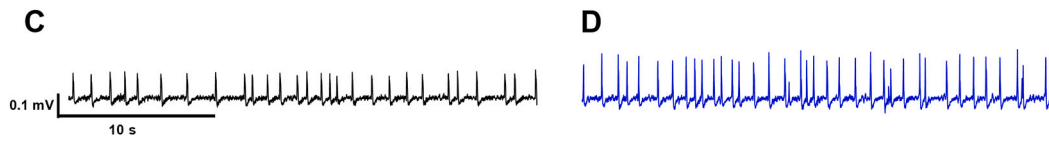
For determining neurodegeneration in the hippocampus, three thionin-stained brain sections (at −1.34, −1.70 and − 2.06 mm AP from bregma) were semi-quantitatively scored using a scoring system described by Gröticke et al. (2008). The left and right hippocampi were scanned in a quasi-random fashion and scores were noted for each of the subregions of the hippocampal formation (CA1, CA2, CA3a, Ca3c, and hilus): score 0 = no obvious damage; score 1 = abnormal appearance of the structure without clear evidence of visible neuronal loss; score 2 = moderate neurodegeneration (lesions involving 20–50% of neurons); score 3 = severe neurodegeneration (lesions involving over 50% of neurons). Furthermore, the extent of the granule cell dispersion (GCD) in the dentate gyrus was visually assessed with a score system: score 0 = no GCD, score 1 = mild GCD, score 2 = moderate GCD, score 3 = severe GCD (Schidlitzki et al., 2017).

Compared to the extent of cell loss occurring after an SE in CA3c and CA1, which can be easily scored by microscopic examination, loss of neurons in the dentate hilus is more difficult to assess without cell counting. Therefore, in a second step, polymorphic neurons (i.e., mossy cells and interneurons) were counted in the dentate hilus of the hippocampal formation. Apart from size, neurons were clearly identifiable on morphological grounds. Neuronal loss was quantified in the ipsilateral hilus at −1.70 mm AP from bregma). The hilus was defined as the inner border of the granule cell layer and two straight lines connecting the tips of the granule cell layer and the proximal end of the CA3c region. All

Baseline activity
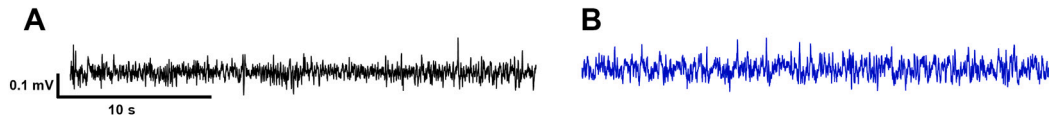
A

B

0.1 mV

10 s

Status epilepticus

C

D

0.1 mV

10 s

High-voltage sharp waves (HVSWs)

E

F

0.1 mV

10 s

G

H

0.1 mV

2 s

Hippocampal paroxysmal discharges (HPDs)

I

J

0.1 mV

10 s

K

L

0.1 mV

2 s
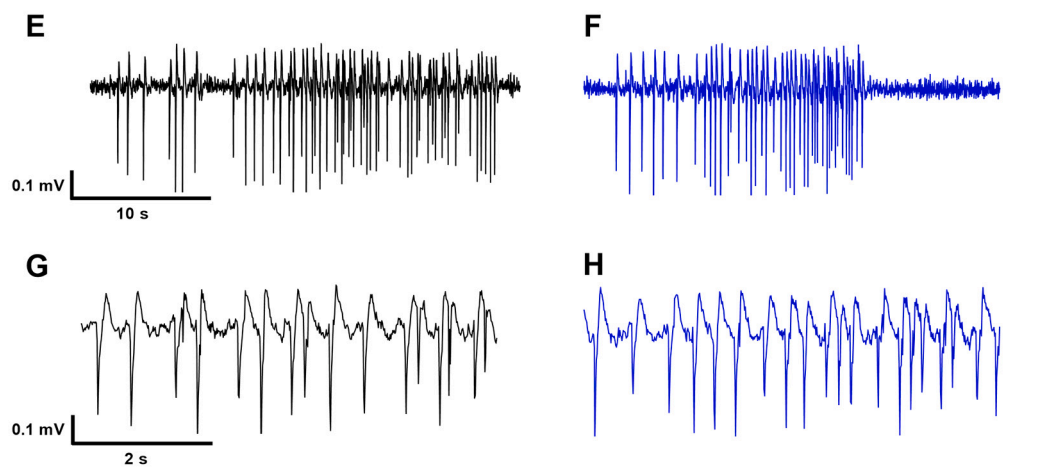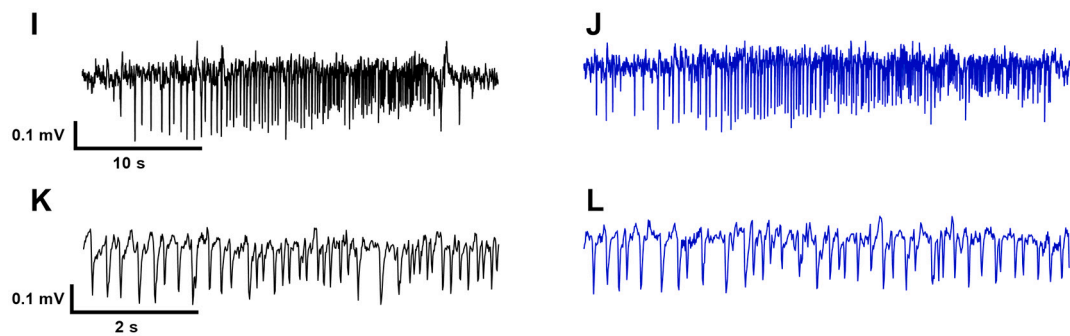
Electroclinical seizures (stage V)

M

N

1 mV

10 s
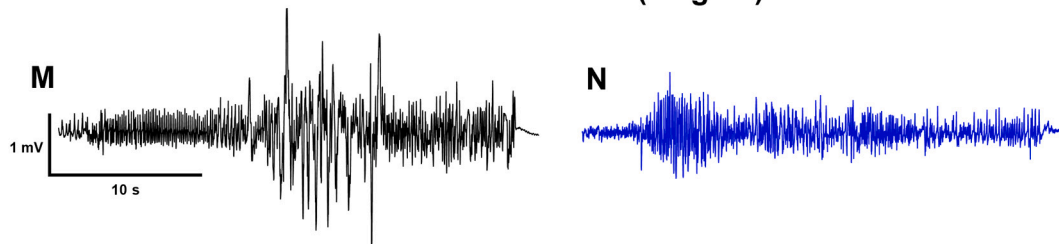
(caption on next page)

Fig. 2. Representative EEG recordings following intrahippocampal injection of kainate in homozygous $Nkcc1^{-/-}$ mice (shown in blue) and wildtype (WT) littermates (shown in black). All recordings were performed via a depth electrode in the hippocampal kainate focus. A: Control hippocampal EEG before injection of kainate in a WT mouse. Note the typical theta oscillations (5–9 Hz), which disappeared during SE in both genotypes. B: Normal hippocampal EEG before injection of kainate in an *Nkcc1* KO mouse. C: Typical paroxysmal EEG activity during status epilepticus (SE) in a WT mouse. D: Typical paroxysmal EEG activity during SE in an *Nkcc1* KO mouse. E: Typical electrographic seizure of the high-voltage sharp wave (HVSW) type in a WT mouse. F: HVSW-type electrographic seizure in an *Nkcc1* KO mouse. G and H: Higher resolution of the HVSWs shown in E and F. I: Typical electrographic seizure of the hippocampal paroxysmal discharge (HPD) type in a WT mouse. J: HPD-type electrographic seizure in an *Nkcc1* KO mouse. K and L: Higher resolution of the HPDs shown in I and J. M: Spontaneous generalized convulsive (score 5) electroclinical seizure in a WT mouse. N: Spontaneous generalized convulsive (score 5) electroclinical seizure in an *Nkcc1* KO mouse. Note that the maximal amplitude of spikes during electroclinical seizure in M and N was much higher than the maximal amplitude of HVSWs and HPDs, so that the scale bars for amplitude (mV) in M and N are different from the scale bars in E-L. Neither the morphology of EEG alterations during SE nor the morphology of spontaneous electrographic or electroclinical seizures differed between WT and *Nkcc1* KO mice. All EEG alterations and associated videos are also shown for both genotypes in movie S1.

cells within these borders were counted at a 200× magnification (Axioscope, Carl Zeiss, Germany). The area of each hilus counted was measured with the KS400 software (Carl Zeiss). Neuronal densities (neurons per unit area) were calculated on the basis of neuronal counts in the hilus and the measured area of the hilus. All neuron counts and area measurements were performed by a person who was blinded with respect to the origin of the sections. In addition to hilus area, the area of the contralateral hippocampus was measured morphometrically at AP -1.70 mm in each mouse to determine whether the size of the hippocampus differed between WT and KO mice (the contralateral hippocampus is not affected by unilateral kainate injection in this model).

We also thought about performing immunohistochemical analysis of the hippocampal expression of NKCC1 following kainate in WT mice, but, unfortunately, to the authors' best knowledge, there are no commercially available NKCC1 antibodies that have been demonstrated to yield a fully NKCC1-specific signal in brain parenchyma by using *Nkcc1* KO brain tissue as controls (see Fritschy, 2008). In fact, this explains much of the inconsistencies in the literature on NKCC1 expression patterns in the brain (Virtanen et al., 2020). Thus, we decided to study the hippocampal expression of NKCC1 mRNA following kainate in WT mice by qPCR (see next section).

2.6. Quantitative real-time polymerase chain reaction (qPCR)

Levels of NKCC1 and KCC2 mRNA expression were quantified in ipsilateral hippocampi after kainate injection compared to sham injected (NaCl) mice by reverse transcription and quantitative real time PCR. Briefly, WT mice (12 weeks of age) were killed by cervical dislocation 24 h after kainate injection and brains were cut at the AP location of the kainate injection site. Total RNA was extracted from anterior part of the ipsilateral hippocampus using RNeasy Plus Mini Kit (Qiagen, Hilden, Germany) and defined amounts (210 ng RNA) were reverse-transcribed into single stranded cDNA using the iScript RT Supermix for RT-qPCR (Bio-Rad, München, Germany) according to the manufacturer's instructions. Quantitative real-time PCR was performed using TaqMan Fast Advanced PCR Master Mix (Thermo Fisher Scientific, Bonn, Germany) and Taq man gene expression assays (Thermo Fisher Scientific) for KCC2 (*Slc12a5*, Mm00803929_m1), NKCC1 (*Slc12a2*, Mm01265951_m1) and housekeeping gene β-actin (Actb, Mm00607939_s1). Reaction conditions were as follows: 50 °C for 2 min, 95 °C for 10 min and 45 cycles of 95 °C for 15 s and 52 °C for 30 s. qPCR analysis was performed using a CFX Connect Real-time PCR System (Bio-Rad) and CFX Maestro Software. Expression levels were calculated using the $2^{(-\Delta CT)}$ method (Schmittgen and Livak, 2008) with β-actin as an internal control.

2.7. Statistics

Depending on whether data were normally distributed or not, parametric or nonparametric tests were used for statistical evaluation. For comparison of two independent groups, Student's *t*-test or the Mann-Whitney *U* test were used; for paired comparisons, Student's t-test or the Wilcoxon signed rank were used. In case of more than two groups we used one-way analysis of variance (ANOVA) with *post-hoc* testing and

correction for multiple comparisons. Depending on data distribution, ordinary ANOVA or the Kruskal-Wallis test were used, followed by Dunn's or Holm-Sidak's multiple comparisons tests. For comparison of frequencies in a 2 × 2 table, Barnard's unconditional test (Barnard, 1947) was used, because this test preserves the significance level and generally is more powerful than Fisher's exact test for moderate to small samples (Lydersen et al., 2009). Grubb's test was used to identify outliers (see section 3). Except for Barnard's unconditional test, all statistical analyses were performed with the Prism 8 software from GraphPad (La Jolla, CA, USA). Two-sided tests were used; a $P \leq 0.05$ was considered significant. The statistical tests used for analyzing the data are described in figure and table legends.

For estimation statistics, analyses were done as described by Ho et al. (2019). We directly introduced the raw data in https://www.estimationstats.com/ and downloaded the results and graphs. In respective graphs, the mean difference for two comparisons is shown with Gardner-Altman estimation plot. Each mean was plotted on the lower axes as a bootstrap sampling distribution. Five thousand bootstrap samples were taken; the confidence interval was bias-corrected and accelerated.

3. Results

3.1. Phenotype of the Nkcc1⁻/⁻ mice vs. WT littermates

Generation of enough WT and homozygous NKCC1 mice from heterozygous mating proved to be extremely difficult, which may be related to the infertility of the homozygous *Nkcc1* KO males (Markadieu and Delpire, 2014). As reported previously (Flagella et al., 1999), homozygous mutants gained body weight well after weaning; however, male homozygous mutants remained smaller as adults (~70% of male wildtype mice), whereas no significant difference in body weight was observed in female adults (Fig. 3A). Furthermore, as reported previously (Flagella et al., 1999), $Nkcc1^{-/-}$ mice frequently exhibited unusual head postures, in which the head was tilted to one side or tilted upward and backward with the nose held high. The mutants also exhibited circling behavior accompanied by a tendency to engage in rapid spinning and shivering. WT littermates behaved normally.

In view of the possibility that the lower body weight of $Nkcc1^{-/-}$ mice is associated with a lower brain size that may affect the relative kainate concentration in the injected hippocampus, we measured the size of the hippocampus. Consistent with the differences in body weight, the average area of the hippocampus was ~15% lower in male $Nkcc1^{-/-}$ mice vs. male WT littermates (which would correspond to a 22% difference in the size or volume of the hippocampus), whereas no such differences were observed in female mice (Fig. 3B). Since the dose-effect experiments with kainate in C57BL/6 WT mice did not indicate that a 20% difference in kainate dose would have any effect on induction of SE or incidence of subsequent SRS (see Methods), we decided to use the same intrahippocampal kainate dose (0.23 μg = 0.92 nM) in both genotypes.

3.2. Intrahippocampal kainate model

A total of 59 mice (23 WT kainate, 23 $Nkcc1^{-/-}$ kainate, 13 WT sham

A

Body weight
(at time of kainate injection)
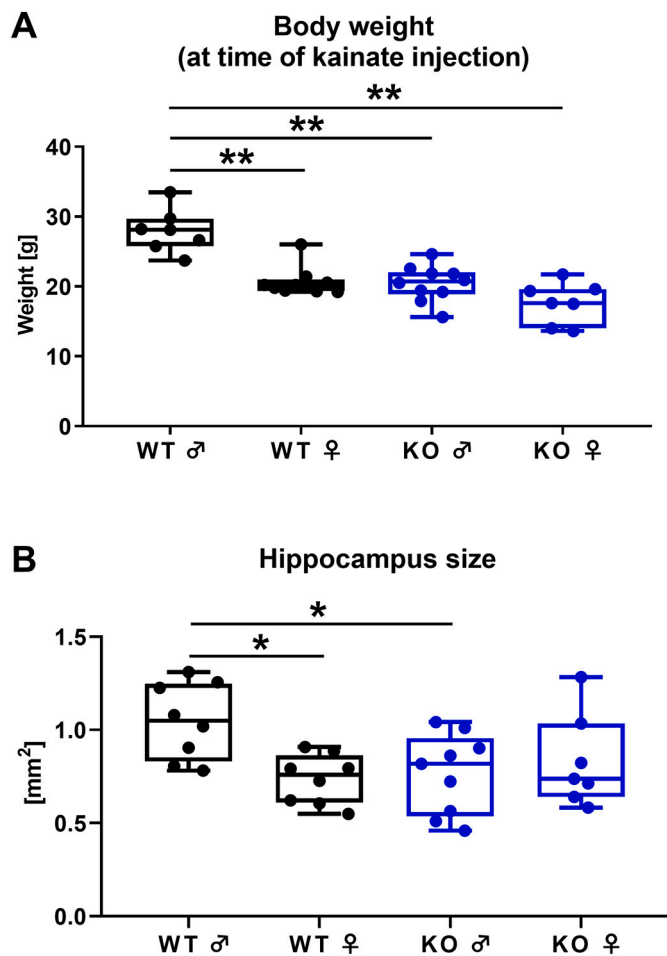

B

Hippocampus size

Fig. 3. Body weight at time of intrahippocampal kainate injection (A) and size of the hippocampus (B) in homozygous $Nkcc1^{-/-}$ mice and wildtype (WT) littermates. Mice were 10-15 weeks of age at time of intrahippocampal kainate injection. The size of the contralateral hippocampus (at −1.34 mm from bregma) was measured at the end of the experimental period illustrated in Fig. 1. Data from both sexes are shown for each genotype. Data are shown as boxplots with whiskers from minimum to maximal values; the horizontal line in the boxes represents the median value. In addition, individual data are shown. Significant group differences are indicated by asterisks (*$P < 0.05$; **$P < 0.0001$). Because data were normally distributed, ordinary one-way ANOVA with posthoc testing by Holm-Sidak's multiple comparisons test were used for statistical analyses.

controls) was used for these experiments. Sex distribution and losses of mice during surgery and SE are shown in Table 2. Final group size for comparison of epileptogenesis was 16 WT and 17 KO mice. However,

Table 2
Group size in the intrahippocampal kainate model. Group differences were analyzed by Barnard's test; see text for results (no significant inter-group differences were found).

Group size	Wildtype littermates	$Nkcc1^{-/-}$
Initial	23 (11 males, 12 females)	23 (13 males, 10 females)
Mortality during anesthesia	1 (female)	0
Mortality during or after SE	1 (male)	5 (3 males, 2 females)
No SE (not used for final analysis of epilepsy)	5 (3 males, 2 females)	1 (female)
Final group size for comparison of kainate-induced epileptogenesis	16 (7 males, 9 females)	17 (10 males, 7 females)

some mice lost their electrode head assembly during the 3 months of the experiment, so that group size differed between the video-EEG monitoring periods at 4-5 and 12-13 weeks illustrated in Fig. 1.

3.2.1. Status epilepticus

Before injection of kainate, hippocampal EEG recordings generally showed typical theta oscillations (5–9 Hz) without obvious differences in WT vs. KO mice (Fig. 2A,B and movie S1). Following injection of kainate (0.23 μg) under anesthesia with chloral hydrate, it took about 5-7 h on average before SE started (see Fig. 4A). As reported previously by us and other groups in studies on different mouse strains (Riban et al., 2002; Maroso et al., 2011; Twele et al., 2016a, 2016b), the limbic SE induced by kainate was characterized by continuous activity of spikes or spike-and-waves and polyspikes in the ipsilateral hippocampal EEG (Fig. 2C,D and movie S1). Mice were either immobile or exhibited clonic movements of the forelimbs; furthermore, in several of the mice intermittent generalized convulsive seizures (Racine stage 3, 4, or 5) were observed; these were associated with concomitant high frequency spikes or polyspikes in the hippocampal recordings. Average SE duration was about 5-6 h (Fig. 4B).

Five of the 22 WT mice did not develop SE after kainate compared to 1/23 KO mice ($P = 0.0758$). As shown in Table 2, mortality during or after SE was 1/17 in WT and 5/22 KO, which was not significantly different ($P = 0.178$). Mice without SE were not used for analysis of epileptogenesis (see below).

When comparing latency to SE and SE duration in WT vs. $Nkcc1^{-/-}$ mice in pooled data on male and female animals, no significant differences were observed (Fig. 4A, B). In addition to continuous nonconvulsive (limbic) seizure activity during SE, intermittent electroclinical seizures (stage 3-5) were observed in both mouse genotypes during SE. Such seizures were observed in 67% of KO vs. 50% of WT mice ($P = 0.333$). Median number of such seizures was 1.5 (range 0-41) in $Nkcc1^{-/-}$ mice vs. 0.5 (range 0-3) in WT mice ($P = 0.0276$; Fig. 4E), indicating that the SE was more severe in the KO mice compared to WT littermates. Interestingly, in terms of seizure frequency during SE, a bimodal distribution was observed in the KO mice, with five mice exhibiting a much higher number of seizures than the rest of the group (Fig. 4E). The incidence and frequency of electroclinical seizures during SE in individual animals are also illustrated in a heat map (Fig. S1). The severity of clinical seizures recorded during SE did not significantly differ between genotypes (Fig. 4F). Notably, however, stage 5 seizures were almost exclusively observed in the KO mice.

With respect to sex differences, female WT mice exhibited a significantly longer latency to SE than male WT mice ($P = 0.0081$; Fig. 4C), whereas no significant sex difference was seen in $Nkcc1^{-/-}$ mice. The latency to SE onset was significantly higher in male $Nkcc1^{-/-}$ mice than in male WT mice, whereas such a genotype difference was not observed in females (Fig. 4C). No significant sex differences within each genotype were observed in SE duration (Fig. 4D) or in the severity of clinical seizures during SE. In male $Nkcc1^{-/-}$ mice, the number of clinical seizures during SE (9.8 ± 4.5) was significantly higher than the number of such seizures in male WT mice (0.57 ± 0.3; $P = 0.0469$), whereas no such difference was observed in female mice (4 ± 2.8 vs. 0.89 ± 0.35; $P = 0.3339$), indicating a sex difference.

3.2.2. Increase of hippocampal NKCC1 mRNA following SE

Whether an SE induced by intrahippocampal injection of kainate in mice enhances the hippocampal expression of NKCC1 is not known. In the pilocarpine model, Li et al. (2008) reported a maximum increase of NKCC1 mRNA in the hippocampus at 24 h after SE.

Twenty-four h after intrahippocampal kainate injection in WT mice, a significant about 4-fold increase in NKCC1 mRNA expression was determined in the ipsilateral hippocampus (Fig. S2A), while KCC2 mRNA expression was not altered (Fig. S2B). Thus, the present model makes it possible to compare the progression and manifestation of epilepsy in the WT animals, where NKCC1 upregulation takes place
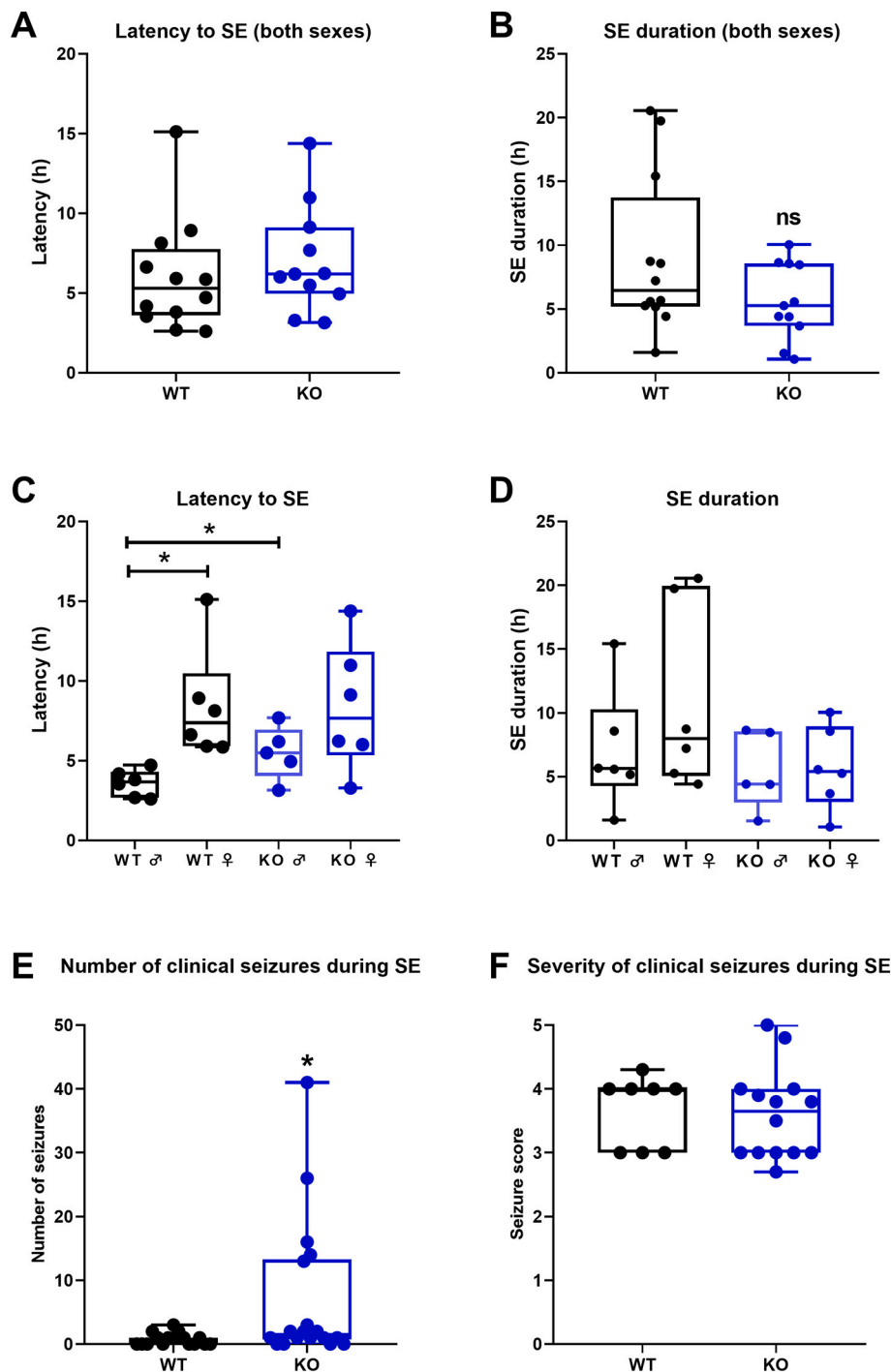
Fig. 4. Characteristics of status epilepticus (SE) in homozygous *Nkcc1*$^{-/-}$ mice and wildtype (WT) littermates. Data are shown as boxplots with whiskers from minimum to maximal values; the horizontal line in the boxes represents the median value. In addition, individual data are shown. Because of disturbances in EEG derivation and technical problems with some of the video recordings, not all mice could be used for final analysis of data, accounting for the lower sample size compared to Table 2. Significant group differences are indicated by asterisks (*$P < 0.05$). For statistical analyses, the Mann-Whitney U test was used for the data in A, B, E, D, and F while data in C and D were analyzed by nonparametric ANOVA (Kruskal-Wallis test) with posthoc Dunn's multiple comparisons test. A: Latency to onset of SE after kainate injection. Kainate was injected into the hippocampus under anesthesia with chloral hydrate, which explains the long latency to SE onset. B: SE duration, as determined by the hippocampal EEG. C and D: SE latency and duration calculated separately for males and females. E: Number of clinical seizures during SE. Typically, the SE after intrahippocampal kainate was nonconvulsive (limbic), but intermittent electroclinical seizures were observed in 50% (wildtype) or 67% (KO) of the mice. Note the bimodal distribution of clinical seizures in the KO mice in that five mice exhibited a higher number of seizures than the rest of the group. F: Average severity of the electroclinical seizures illustrated in E. In each mouse, the severity of electroclinical seizures was averaged and used for the group data illustrated in this figure.

promptly after SE, with the KOs that have no NKCC1 at all.

3.2.3. Latency to onset of spontaneous seizures after SE

As described by Heinrich et al. (2011) and us (Twele et al., 2016a) previously, following spontaneous termination of SE, the hippocampal EEG may return to basal activity, interrupted by few low voltage spikes. Onset of epilepsy following such latent period is indicated by the occurrence of spontaneous electrographic seizures, typically first HVSWs and then HPDs, which may progress into electroclinical seizures (Heinrich et al., 2011; Twele et al., 2016a). As reported previously for C57BL/6 mice (Ndode-Ekane and Pitkänen, 2013; Twele et al., 2016a), when electrographic seizures were used to indicate the onset of epilepsy, almost no seizure-free latent period was observed in the WT mice. A

similar observation was made in the KO mice. Average latent period was 25.1 h (range 0–158 h) in WT vs. 23.1 h (0–57 h) in KO mice, respectively. All data were also separately calculated for male and female mice; no significant sex differences were observed (cf., Fig. S1).

3.2.4. Incidence and frequency of spontaneous electrographic seizures after SE

The incidence of SRS was determined by continuous (24/7) video-EEG monitoring at 4-5 and 12-13 weeks after kainate (see Fig. 1). As illustrated in Fig. 5A, 77% of WT mice exhibited spontaneous recurrent electrographic seizures (HVSWs and/or HPDs) at 4-5 weeks after kainate. Median frequency of such seizures was 11/h (Fig. 5C). At 12-13 weeks after kainate (Fig. 5B,D), the median frequency of electrographic
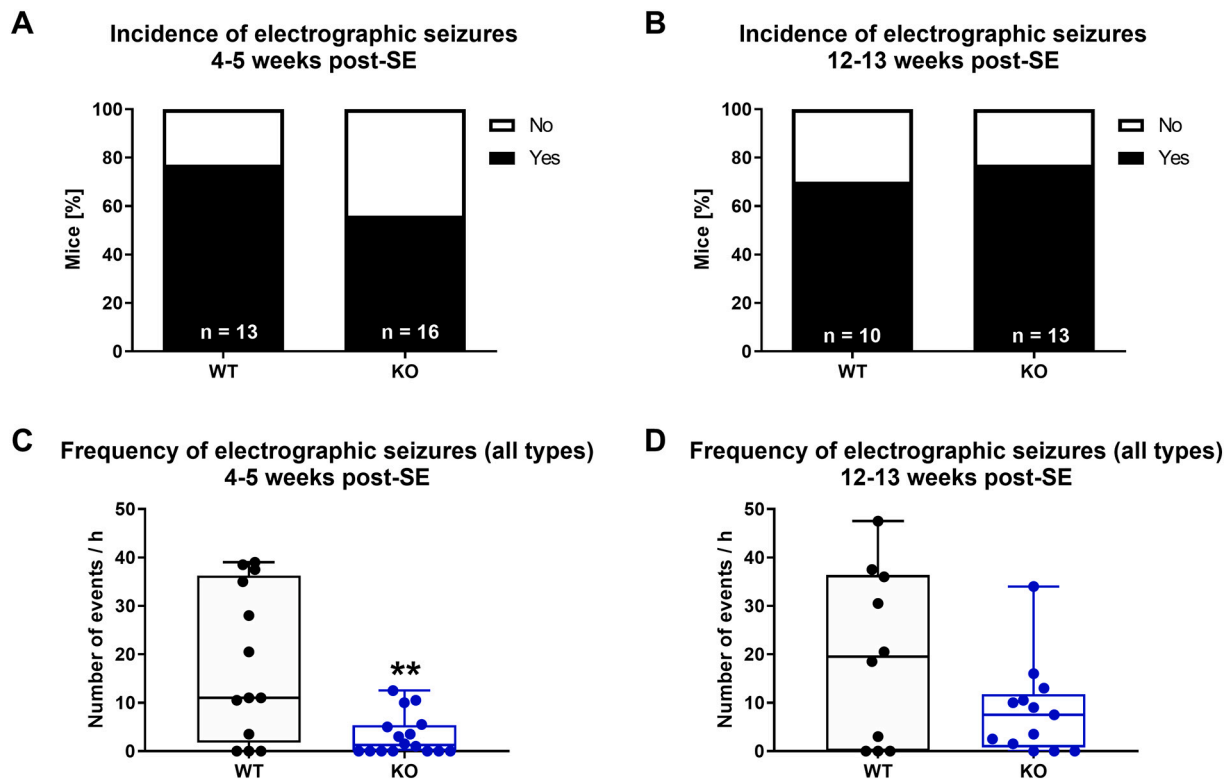
Fig. 5. Incidence and frequency of spontaneous electrographic seizures recorded at 4-5 and 12-13 weeks after intrahippocampal kainate injection in homozygous *Nkcc1*$^{-/-}$ mice and wildtype (WT) littermates. In A and B, incidence of electrographic seizures is shown as percentage, whereas seizure frequencies illustrated in C and D are shown as boxplots with whiskers from minimum to maximal values; the horizontal line in the boxes represents the median value. In addition, individual data are shown. Sample size is 13 WT and 16 KO mice at 4-5 weeks and 10 WT and 13 KO mice at 12-13 weeks, respectively. Because of disturbances in EEG derivation or loss of electrode assemblies, not all mice could be used for final analysis of data, explaining the lower sample size compared to Table 2. Furthermore, some mice lost their electrode assemblies between the 4 and 12 weeks recording periods, resulting in the lower sample size at 12 weeks. Significant group differences are indicated by asterisks (**$P < 0.01$). For statistical analyses, Barnard's test was used for the incidence data in A and B, while frequency data in C and D were analyzed by the Mann-Whitney *U* test. A: Incidence of electrographic seizures (HVSWs and HPDs) at 4-5 weeks after status epilepticus (SE). B: Incidence of electrographic seizures (HVSWs and HPDs) at 12-13 weeks after SE. C: Frequency of electrographic seizures (HVSWs and HPDs) at 4-5 weeks after SE. D: Frequency of electrographic seizures (HVSWs and HPDs) at 12-13 weeks after SE. All data were also separately calculated for male and female mice; no significant sex differences were observed (not shown).

seizures (19.5/h) was not statistically different ($P = 0.5519$). The individual frequency of electrographic seizures in WT and KO mice at 4-5 and 12-13 weeks after kainate is also shown in a heat map (Fig. S1). When HVSWs and HPDs were analyzed separately in WT mice, the median frequency of HVSWs was 10.5/h at 4-5 weeks and 15.8/h at 12-13 weeks ($P = 0.5781$), whereas the median frequency of HPDs was 0.5/h at 4-5 weeks and 1/h at 12-13 weeks ($P = 0.3828$), respectively.

As shown in Fig. 5A,B, the incidence of electrographic SRS was not significantly different in *Nkcc1*$^{-/-}$ mice. However, the frequency of electrographic seizures was significantly lower in *Nkcc1*-KO vs. WT mice at 4-5 weeks after SE (Fig. 5C).

Both the incidence and frequency of HVSWs were higher than those of HPDs in WT mice (Fig. 6A-F). The incidence of HVSWs was not different between WT and KO mice at both 4-5 or 12-13 weeks after kainate; however, at 12-13 weeks the incidence of HPDs was significantly lower in KO than WT mice (Fig. 6D). The frequency of HVSWs was significantly lower in KO mice at 4-5 weeks after kainate (Fig. 6E), accounting for the lower frequency of electrographic seizures illustrated in Fig. 5C. Furthermore, the frequency of HPDs was significantly lower at 12-13 weeks after SE (Fig. 6F). Finally, all the data above were separately calculated for male and female mice, but no significant sex differences were observed (not shown).

3.2.5. Incidence and frequency of spontaneous electroclinical seizures after SE

As shown in Fig. 7A, 75% of WT mice exhibited spontaneous

recurrent electroclinical seizures at 4-5 weeks after kainate. Median frequency of such seizures was 2.5 per week (Fig. 7C). However, at 12-13 weeks after kainate, the incidence of electroclinical seizures significantly decreased to 33% ($P = 0.0147$ vs. 4-5 weeks) (Fig. 7B). Furthermore, median frequency of such seizures in WT mice significantly decreased from 2.5 seizures per week (range 0-25) at 4-5 weeks to 0 seizures per week (range 0-81) at 12-13 weeks ($P = 0.0171$)(Fig. 7D). As shown in Fig. 7D, 12/13 WT mice had a seizure frequency around zero. One WT mouse in this group exhibited a very high seizure frequency (~80 seizures per week) and turned out to be a statistical outlier (see legend to Fig. 7).

In *Nkcc1*$^{-/-}$ mice, incidence and frequency of electroclinical seizures were not significantly different from WT mice at 4-5 weeks after kainate (Fig. 7A, C; but see section 3.2.7). However, at 12-13 weeks after kainate, both incidence and frequency of electroclinical seizures were significantly higher compared to WT controls (Fig. 7B, D), indicating a pro-epileptogenic effect of NKCC1 deletion. The individual distribution of electroclinical seizures over the two one-week periods of continuous video/EEG monitoring is illustrated in Fig. S1. All data were also separately calculated for male and female mice; no significant sex differences were observed (cf., Fig. S1). Three mice (one WT, two KO) died during the chronic phase of epilepsy as shown in Fig. S1.

3.2.6. Comparison of epilepsy in Nkcc1$^{-/-}$ mice with few vs. numerous clinical seizures during SE

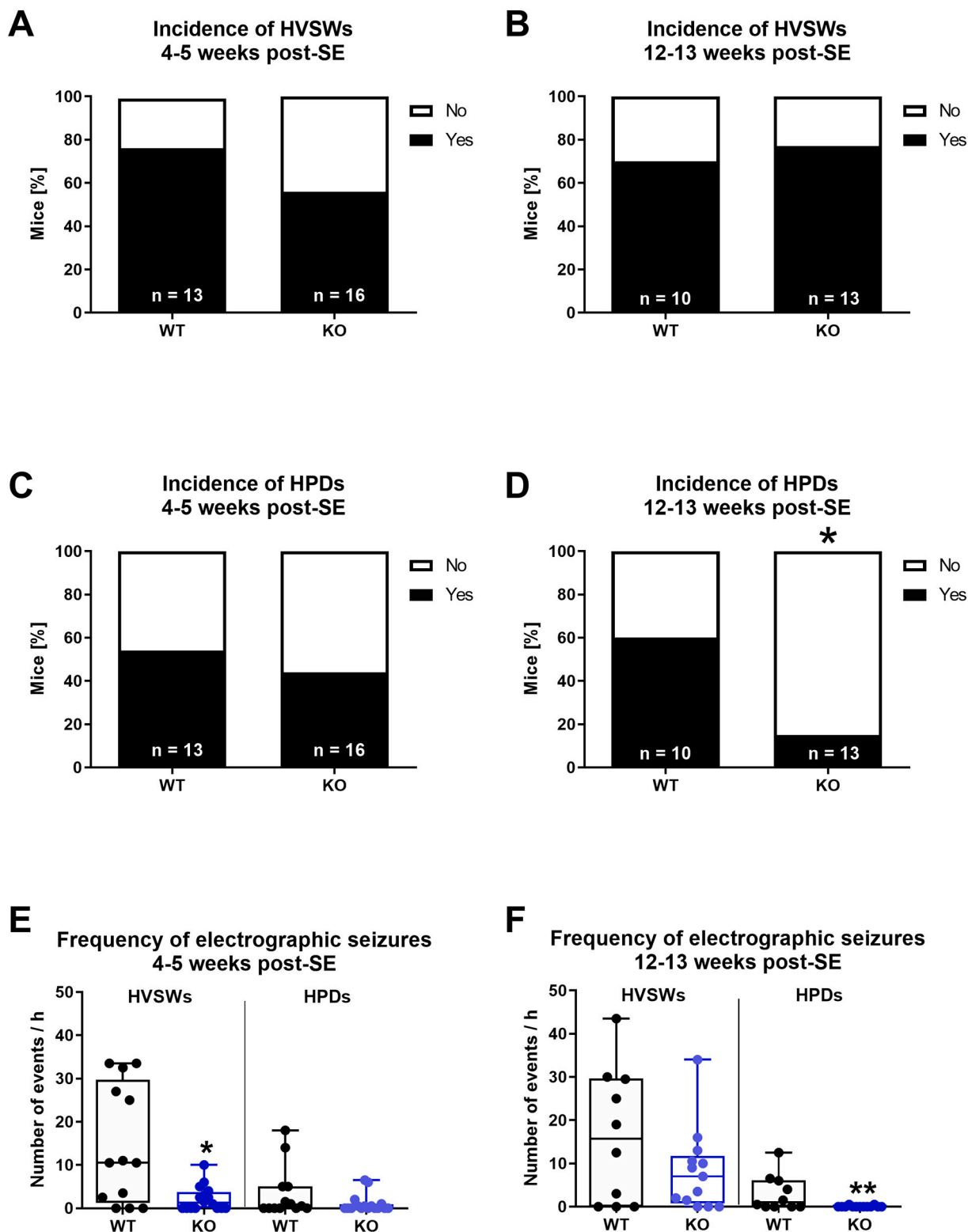As described in 3.2.1 and shown in Fig. 4E and S1, two subgroups of

Fig. 6. Incidence and frequency of spontaneous electrographic seizures (separately shown for HVSWs and HPDs) recorded at 4-5 and 12-13 weeks after intra-hippocampal kainate injection in homozygous *Nkcc1$^{-/-}$* mice and wildtype (WT) littermates. In A-D, incidence of electrographic seizures is shown as percentage, whereas seizure frequencies illustrated in E and F are shown as boxplots with whiskers from minimum to maximal values; the horizontal line in the boxes represents the median value. In addition, individual data are shown. See Fig. 5 legend for details on sample size. Significant group differences are indicated by asterisks (*$P <$ 0.05; **$P <$ 0.01). For statistical analyses, Barnard's test was used for the incidence data in A, B, C, and D, while frequency data in E and F were separately analyzed for HVSWs and HPDs by the Mann-Whitney U test. A: Incidence of HVSWs at 4-5 weeks after status epilepticus (SE).). B: Incidence of HVSWs at 12-13 weeks after SE. C: Incidence of HPDs at 4-5 weeks after status epilepticus (SE).). D: Incidence of HPDs at 12-13 weeks after SE. E: Frequency of HVSWs and HPDs at 4-5 weeks after SE. F: Frequency of HVSWs and HPDs at 12-13 weeks after SE. All data were also separately calculated for male and female mice; no significant sex differences were observed (not shown).
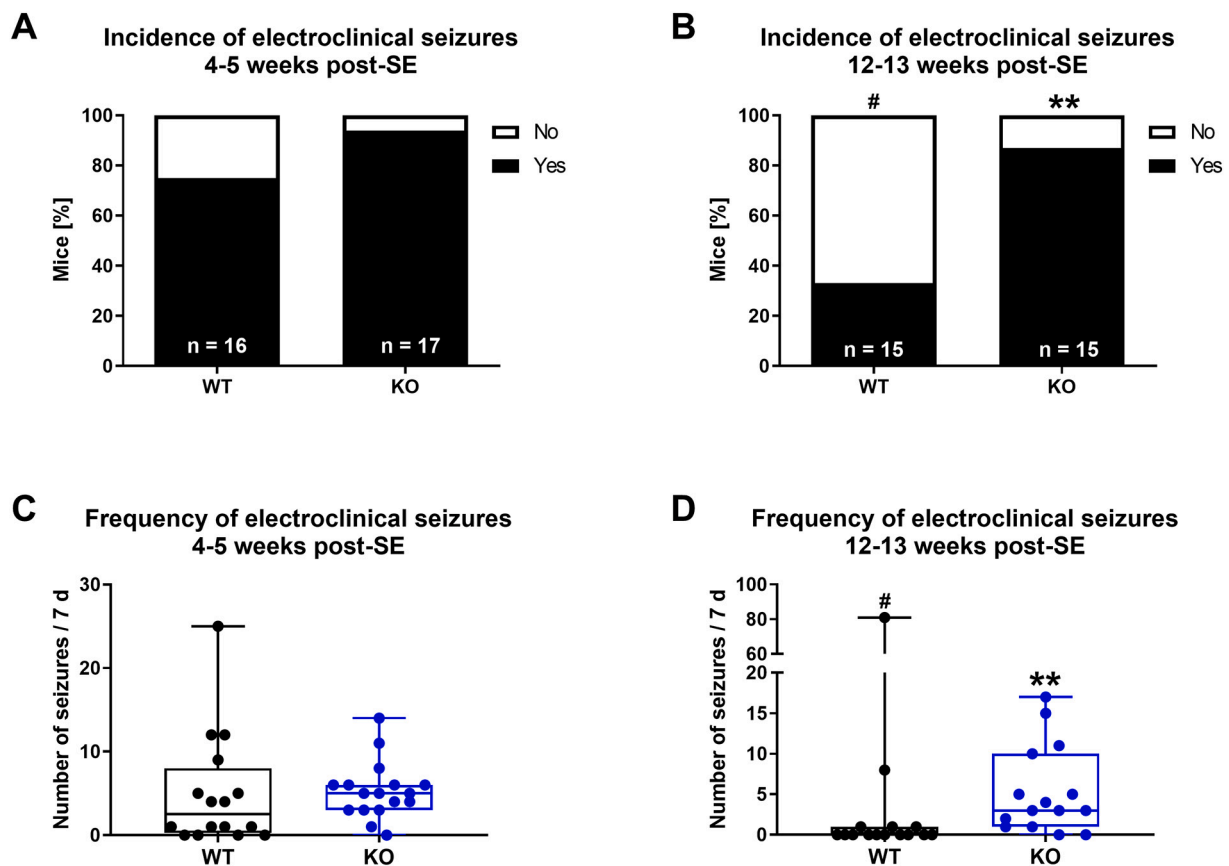
Fig. 7. Incidence and frequency of spontaneous electroclinical seizures recorded at 4-5 and 12-13 weeks after intrahippocampal kainate injection in homozygous *Nkcc1*$^{-/-}$ mice and wildtype (WT) littermates. In A and B, incidence of electrographic seizures is shown as percentage, whereas seizure frequencies illustrated in C and D are shown as boxplots with whiskers from minimum to maximal values; the horizontal line in the boxes represents the median value. In addition, individual data are shown. Sample size is 16 WT and 17 KO mice at 4-5 weeks and 15 WT and 15 KO mice at 12-13 weeks, respectively. Significant differences between *Nkcc1*$^{-/-}$ mice and WT littermates are indicated by asterisks ($*P < 0.05$; $**P < 0.01$), whereas significant differences within each group between the data at 12 vs. 4 weeks are indicated by the hash sign ($^{\#}P < 0.05$). For statistical analyses, Barnard's test was used for the incidence data in A and B, while frequency data in C and D were analyzed by the Mann-Whitney U test. Differences within each group between the data at 12 vs. 4 weeks in C and D were analyzed by the Wilcoxon signed rank test. A: Incidence of electroclinical seizures at 4-5 weeks after status epilepticus (SE). A: Incidence of electroclinical seizures at 12-13 weeks after SE. C: Frequency of electroclinical seizures 4-5 weeks after SE. D: Frequency of electroclinical seizures at 12-13 weeks after SE. Note that Grubb's test indicated that the WT mouse with 81 seizures per week in D is an outlier (see also Fig. S3D). All data were also separately calculated for male and female mice; no significant sex differences were observed (not shown).

Nkcc1 KO mice could be distinguished in terms of number of convulsive seizures during SE: (i) KO mice with no or few (1-2) seizures, and (ii) KO mice with numerous (13-41) seizures. We analyzed these two subgroups separately in order to test whether they differed in the *consequences* of SE. As shown in Figs. S1 and S3, no significant differences were found. The incidence of electrographic seizures (Fig. S3A) and electroclinical seizures (Fig. S3E) tended to be higher in the subgroup with the more severe SE, but the difference was not statistically significant. Furthermore, the severity of neuronal damage in CA1 and CA3c was the same in both subgroups (see below). Thus, increased SE severity was not the cause of the more severe epilepsy phenotype in *Nkcc1* KO mice.

3.2.7. Calculation of effect size of intergroup differences in frequency of spontaneous seizures by estimation statistics

In addition to the traditional presentation of data on seizure frequencies, we used estimation statistics and graphics to visualize effect sizes. The primary aim of estimation statistics is to report an effect size along with its confidence interval, the latter of which is related to the precision of the estimate (Ho et al., 2019). As shown in Fig. 8A,B, estimation statistics indicated a similar effect size for the decrease in frequency of electrographic seizures in *Nkcc1* KO mice vs. WT littermates at both 4-5 and 12-13 weeks after SE. On the contrary, at both time points electroclinical seizures increased with similar effect size in *Nkcc1* KO

mice vs. WT littermates. Thus, the estimation graphics in Fig. 8 indicate that at both 4-5 and 12-13 weeks, there was enhanced progression from electrographic to electroclinical seizures in *Nkcc1* KO mice compared to WT littermates.

3.2.8. Severity and duration of spontaneous electroclinical seizures after SE

As shown in Fig. S4A, most spontaneous electroclinical seizures were secondarily generalized convulsive (stage 5) seizures. Seizure severity did not differ significantly between WT and KO mice. The average duration of electroclinical seizures was ~45 s at both 4-5 weeks and 12-13 weeks after SE without any significant inter-group differences in the WT and KO mice (Fig. S4B). All data were also separately calculated for male and female mice; no significant sex differences were observed (not shown).

3.2.9. Histological alterations following SE

As reported previously (Bouilleret et al., 1999; Riban et al., 2002), intrahippocampal kainate injection and the resulting SE caused severe neuropathological changes in the ipsilateral hippocampus, being characterized by almost complete loss of pyramidal neurons in the CA1 and CA3c layers and a marked GCD when examined at ~3 months after kainate injection (Fig. 9). No alterations were observed in the contralateral hippocampus. When the severity of the changes in the ipsilateral
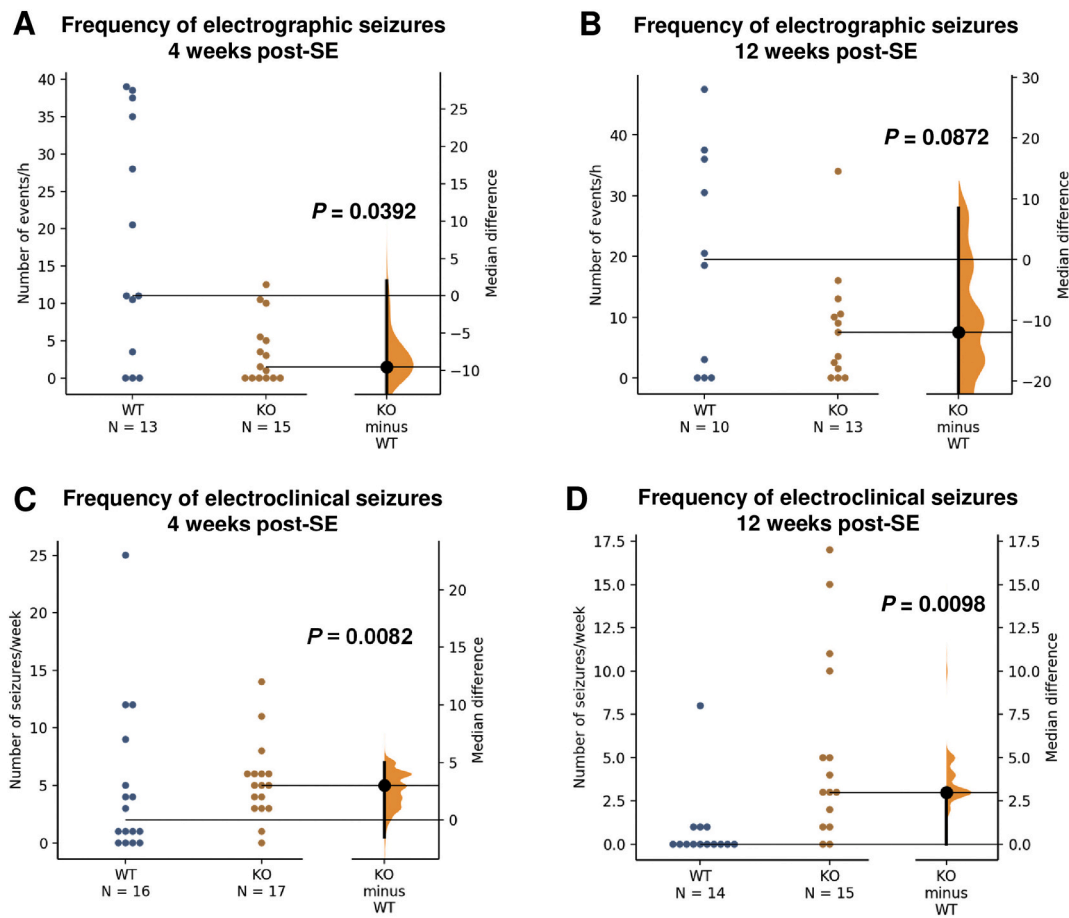
Fig. 8. Different frequencies of spontaneous recurrent seizures in WT vs. *Nkcc1* KO mice as analyzed with estimation statistics. In each graph, the median differences between WT and KO are shown in the Gardner-Altman estimation plots. Both groups are plotted on the left axes; the mean difference is plotted on a floating axis on the right as a bootstrap sampling distribution. The mean difference is depicted as a dot; the 95% confidence intervals are indicated by the ends of the vertical error bars. A: Frequency of electrographic seizures at 4-5 weeks after kainate. The unpaired median difference between 0 and KO is −9.5 [95.0%CI -28.0, 2.0]. The *P* value of the two-sided permutation *t*-test is 0.0392. B: Frequency of electrographic seizures at 12-13 weeks after kainate. The unpaired median difference between WT and KO is −12.0 [95.0%CI -31.8, 8.5]. The *P* value of the two-sided permutation t-test is 0.0872. C: Frequency of electroclinical seizures at 4-5 weeks after kainate. The unpaired median difference between WT and KO is 3.0 [95.0%CI -1.5, 5.0]. The *P* value of the two-sided permutation t-test is 0.0082. D: Frequency of electroclinical seizures at 12-13 weeks after kainate. For the data in D, one outlier (see Fig. 7D) was removed by the method of Grubb. The unpaired median difference between WT and KO is 3.0 [95.0%CI 0.0, 3.0]. The *P* value of the two-sided permutation t-test is 0.0098. If the potential outlier is not deleted, the unpaired median difference between WT and KO is 3.0 [95.0%CI 0.0, 3.0]. The *P* value of the two-sided permutation t-test is 0.0098. Thus, the potential WT outlier does not affect the analysis of the group difference.

hippocampus was scored, no significant differences between WT and *Nkcc1*-KO mice were observed for neurodegeneration in CA1 and CA3c (Fig.10A,B) or GCD (Fig. 10C). When neurons in the dentate hilus were counted, comparable neuronal numbers and densities were obtained for WT and *Nkcc1*-KO mice after kainate, which did not significantly differ from sham controls (Fig.10D,F). However, the area of the ipsilateral hilus was significantly increased in WT mice after kainate, which was not observed in *Nkcc1*-KO mice (Fig.10E). All data were also separately calculated for male and female mice; no significant sex differences were observed (not shown).

4. Discussion

Epileptogenesis has been associated with an increased neuronal expression of NKCC1 in several studies (e.g., Li et al., 2008; Koyama et al., 2012; Marguet et al., 2015; Stamboulian-Platel et al., 2016; Kourdougli et al., 2017; Auer et al., 2020; Liu et al., 2020). In the present work, we used *Nkcc1* WT and KO mice in the intrahippocampal kainate model of mesial TLE to address the question whether NKCC1 upregulation in the brain is a necessary condition for the induction and progression of epilepsy. Our present observation of a robust hippocampal

upregulation of NKCC1 in the WT animals within 24 h after SE provides an excellent basis for a meaningful comparison between the two genotypes in the present context.

The main findings of the present study are that (1) homozygous $Nkcc1^{-/-}$ mice exhibit a more severe SE with more generalized convulsive seizures than WT littermates, and (2) epileptogenesis after SE significantly differs between genotypes. Estimation graphics indicated that *Nkcc1* mice exhibit less spontaneous electrographic seizures but more electroclinical seizures than WT mice at both 4-5 and 12-13 weeks after kainate. Thus, surprisingly (see Introduction), the epileptic phenotype of the *Nkcc1* mice is more severe compared to WT mice. More generally, our data suggest that NKCC1 is dispensable for the induction, progression and manifestation of epilepsy.

The progressive evolution of electrographic and electroclinical seizures after intrahippocampal kainate injection in mice has been described previously by several groups, including our own (Riban et al., 2002; Heinrich et al., 2011; Maroso et al., 2011; Twele et al., 2016a; Sandau et al., 2019). During the latent period, the first electrographic signs of seizure activity recorded in the ipsilateral hippocampus are typically HVSWs, followed by HPDs and finally secondarily generalized electroclinical seizures, which subsequently spread to the cerebral
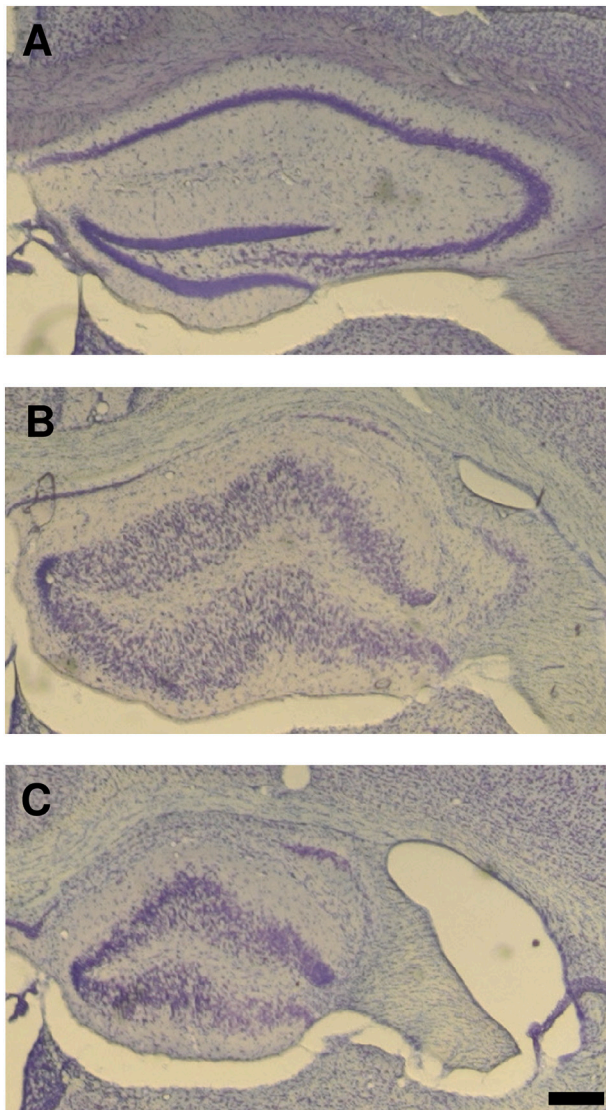
Fig. 9. Photomicrographs of the ipsilateral hippocampus of homozygous $Nkcc1^{-/-}$ mice and wildtype (WT) littermates. Animals were perfused at ~3 months after intrahippocampal kainate injection (or sham injection) and brains were stained with thionin for histological analysis. Shown are representative photomicrographs of ipsilateral hippocampi of (A) a sham-operated WT mouse, (B) a kainate-treated WT mouse, and (C) a kainate-treated $Nkcc1^{-/-}$-mouse. Scale bar = 200 μm. In B and C, the CA1 and CA3c pyramidal cell layers are almost completely damaged. Note the marked granule cell dispersion in both B and C. As reported previously (Bouilleret et al., 1999; Riban et al., 2002; Gröticke et al., 2008; Schidlitzki et al., 2017), no obvious structural changes were seen in the contralateral hippocampi of kainate-injected mice (not shown).

cortex. The present findings thus indicate that NKCC1 deletion leads to increased progression of focal electrographic (nonconvulsive) seizures to secondarily generalized convulsive electroclinical seizures in the chronic phase of epilepsy in this model.

The finding that the incidence and frequency of electroclinical seizures in WT mice was significantly lower at 12-13 vs. 4-5 weeks after kainate was unexpected and may be due to the genetic background of these mice (see Methods), because we did not observe such a difference in another (NMRI) mouse strain (Schidlitzki et al., 2017; Schidlitzki et al., 2020). Remission of electroclinical seizures as determined in the WT mice here was not observed in $Nkcc1^{-/-}$ mice. However, as reported previously by several groups for C57BL/6 and some other mouse strains (Riban et al., 2002; Maroso et al., 2011; Duveau et al., 2016; Schidlitzki

et al., 2017; Sandau et al., 2019; Schidlitzki et al., 2020), the WT mice of the present study exhibited frequent spontaneous electrographic seizures (HVSWs and HPDs) at both early and late time points after kainate, indicating chronic epilepsy. In this respect, it is important to note that most groups using the intrahippocampal kainate model of TLE only monitor the frequent electrographic seizures but not the infrequent electroclinical seizures.

Until recently, it was not known whether an SE induced by intrahippocampal kainate injection increases NKCC1 expression in the hippocampus similar to the changes reported for the pilocarpine model (Li et al., 2008; Brandt et al., 2010; Kourdougli et al., 2017). In the present study, we found that hippocampal NKCC1 mRNA expression of WT mice is significantly (~400%) increased already 24 h after the kainate-induced SE, which is similar to the findings of Li et al. (2008) in the lithium-pilocarpine model in mice. Cell-specific information cannot be obtained by studying NKCC1 mRNA expression in brain tissue samples (Virtanen et al., 2020). With respect to cell-specific labeling of NKCC1 by immunohistochemistry as done in several previous studies in epilepsy models, a serious shortcoming in such studies is the absence of KO-validated immunohistochemical procedures (for review, see Virtanen et al., 2020). This problem is accentuated by the fact that NKCC1 shows a wide distribution in a variety of cells within the brain, including different types of glial cells, brain capillary endothelial cells, and neurons. Moreover, neurons are likely to make a minor contribution to total tissue levels of NKCC1 mRNA and protein (Virtanen et al., 2020). In the $Nkcc1^{-/-}$ mice used here, NKCC1-related alterations can obviously not occur, thus providing a tool to determining the role of NKCC1 in epileptogenesis following intrahippocampal kainate injection, although the limitations of constitutive KO should be kept in mind.

The $Nkcc1^{-/-}$ mice used in these previous and present experiments are conventional (constitutive) KO mice, in which the target gene is permanently inactivated in the germ line and, consequently, in all cells of the animal at all stages of development. One of the main disadvantages of constitutive gene KO is that the deletion could activate compensatory genes that interfere with the readouts examined in the affected mice (Caceres et al., 2018). The global $Nkcc1$ KO has a high degree of mortality at baseline, and therefore the mice that survive may have specific compensatory mechanisms (however, not necessarily within the brain) to overcome the lack of NKCC1. In theory, this might render the surviving animals more susceptible to higher progression of electrographic to electroclinical seizures. Thus, further work is needed on conditional and inducible KO mouse models which allow the activation/inactivation of a target gene at a given time point and within a particular tissue or cell type (Caceres et al., 2018). Tissue-specific, conditional $Nkcc1^{-/-}$ mice have been developed (Antoine et al., 2013), but, to our knowledge, not yet used for studying the role of cell-specific expression of NKCC1 in seizures and epilepsy. When judging the utility of the full KO mouse as used here, it is important to note that the cellular targets of bumetanide's effects on seizures and epilepsy have not been identified sufficiently. Therefore, using cell-specific conditional NKCC1 KO mice at present might not be more advantageous – perhaps the opposite. Thus, we believe that the present findings are highly interesting for a large number of researchers who work on NKCC1 as a potential drug target. Moreover, the present data on the constitutive KO are likely to catalyze work on more specific genetic manipulations, especially as our results raise the somewhat surprising possibility that blocking NKCC1 in the CNS may not be beneficial in the prevention of seizures.

In the present study, the typical neurodegeneration and granule cell dispersion occurring in the ipsilateral hippocampus of the intrahippocampal kainate mouse model (Riban et al., 2002) was not altered by NKCC1 deletion. However, the increased size of the dentate hilus was not observed in NKCC1 KO mice. An increase in hilus area (or volume) is often seen in rodent models of TLE and has been related to edema, but also astrogliosis or ectopic granule cell development (Lassmann et al., 1984; Brandt et al., 2004; McCloskey et al., 2006; Scharfman and Pierce,
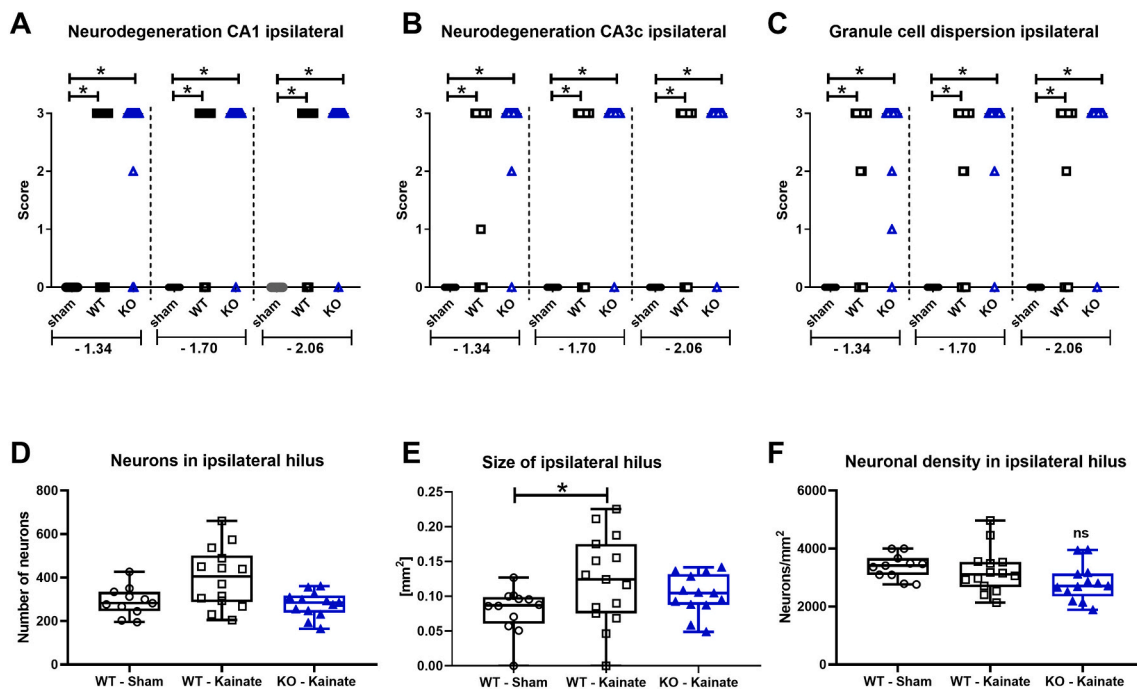
Fig. 10. Hippocampal damage and granule cell dispersion at ~3 months after intrahippocampal kainate injection in homozygous *Nkcc1⁻/⁻* mice and wildtype (WT) littermates. Sham WT mice were used for comparison. Severity of neurodeneration in ipsilateral CA1 (A) and CA3c (B) as well as of granule cell dispersion (C) was scored and is shown as individual values with median. In the ipsilateral dentate hilus, neurons were counted and neuron number (D), hilus area (E), and neuronal density (F) are shown as boxplots with whiskers from minimum to maximal values; the horizontal line in the boxes represents the median value. In addition, individual data are shown. Significant group differences in A-F are indicated by asterisks (*$P < 0.05$). All data were also separately calculated for male and female mice; no significant sex differences were observed (not shown). For statistical analyses, data in A, B, and C were analyzed by nonparametric ANOVA (Kruskal-Wallis test) with posthoc Dunn's multiple comparisons test, whereas data in D, E, and F were analyzed by ordinary one-way ANOVA with posthoc testing by Holm-Sidak's multiple comparisons.

2012). NKCC1 is highly expressed on the luminal membrane of the cerebral vascular endothelium and seems to be critically involved in ionic edema and swelling of the brain parenchyma following brain insults, including SE (Kahle et al., 2009; Simard et al., 2010; Wallace et al., 2011; Mokgokong et al., 2014). In addition, glial expression of NKCC1 is involved in cell swelling (Hochman, 2012). Thus, the function of NKCC1 in brain endothelial and glial cells may explain the lack of increase in hilar volume in response to kainate observed in *Nkcc1⁻/⁻* mice.

The present finding that NKCC1 deletion does not exert antiepileptogenic effects in the intrahippocampal kainate model is in line with previous pharmacological experiments of Nardou et al. (2009), using an *in vitro* preparation composed of two intact interconnected rat hippocampi in a three compartment chamber, in which seizures are induced by kainate in one hippocampus, thus allowing to investigate the effects of drugs on both the seizure propagation to the other hippocampus and seizure-induced epileptogenic mirror focus formation. They reported that inhibition of NKCC1 by bumetanide (10 μM) did not prevent generation of kainate-induced seizures and their propagation to the "drug-naïve" contralateral hippocampus. Bumetanide also failed to prevent the formation of an acute epileptogenic mirror focus in the contralateral hippocampus that had not been exposed to kainate, but only to propagating seizures originating from the drug-exposed hippocampus. These findings demonstrate that blocking NKCC1 activity alone does not prevent epileptogenesis, which is further substantiated by our previous *in vivo* experiments with bumetanide in the rat pilocarpine model (Brandt et al., 2010) and the present experiments with genetic NKCC1 deletion in the intrahippocampal kainate mouse model of TLE.

From a pharmacological point of view, it is important to add in the present context that applying bumetanide at the level of the whole animal or directly into the brain does not, either, provide any information on the likely heterogenous effects mediated by the drug in various kinds of cells and tissues with significant levels of NKCC1 expression (see Russell, 2000; Virtanen et al., 2020). Thus, we feel that our present data on the full *Nkcc1* KO are of much relevance for current and future studies in the present field of research.

In conclusion, despite extensive research, it remains unknown whether changes in NKCC1 and KCC2 expression and function act as protective or adaptive mechanisms during brain injury such as induced by SE or TBI. This important issue should, obviously, deserve much more attention in the interpretation of the effects of NKCC1-targeting drugs in epilepsy and in their possible therapeutic implementation. The present findings in *Nkcc1⁻/⁻* mice do not support the widely held notions that NKCC1 and its upregulation in the brain are closely involved in epileptogenesis and manifestation of epilepsy, and that using inhibitors of NKCC1 is a useful strategy for preventing or modifying epilepsy.

Supplementary data to this article can be found online at https://doi.org/10.1016/j.nbd.2021.105297.

Declaration of Competing Interest

The authors have no conflicts of interest to declare.

Acknowledgements

References

Antoine, M.W., Hübner, C.A., Arezzo, J.C., Hébert, J.M., 2013. A causative link between inner ear defects and long-term striatal dysfunction. Science 341, 1120–1123.

Auer, T., Schreppel, P., Erker, T., Schwarzer, C., 2020. Impaired chloride homeostasis in epilepsy: Molecular basis, impact on treatment, and current treatment approaches. Pharmacol. Ther. 205, 107422.

Barmashenko, G., Hefft, S., Aertsen, A., Kirschstein, T., Köhling, R., 2011. Positive shifts of the GABAA receptor reversal potential due to altered chloride homeostasis is widespread after status epilepticus. Epilepsia 52, 1570–1578.

Barnard, G.A., 1947. Significance tests for 2 X 2 tables. Biometrika. 34, 123–138.

Ben-Ari, Y., 2017. NKCC1 Chloride Importer Antagonists Attenuate Many Neurological and Psychiatric Disorders. Trends Neurosci. 40, 536–554.

Ben-Ari, Y., Khalilov, I., Kahle, K.T., Cherubini, E., 2012. The GABA excitatory/inhibitory shift in brain maturation and neurological disorders. Neuroscientist. 18, 467–486.

Blaesse, P., Airaksinen, M.S., Rivera, C., Kaila, K., 2009. Cation-chloride cotransporters and neuronal function. Neuron 61, 820–838.

Borges, K., Gearing, M., McDermott, D.L., Smith, A.B., Almonte, A.G., Wainer, B.H., Dingledine, R., 2003. Neuronal and glial pathological changes during epileptogenesis in the mouse pilocarpine model. Exp. Neurol. 182, 21–34.

Bouilleret, V., Ridoux, V., Depaulis, A., Marescaux, C., Nehlig, A., Lasalle, G.L., 1999. Recurrent seizures and hippocampal sclerosis following intrahippocampal kainate injection in adult mice: Electroencephalography, histopathology and synaptic reorganization similar to mesial temporal lobe epilepsy. Neuroscience 89, 717–729.

Brandt, C., Ebert, U., Löscher, W., 2004. Epilepsy induced by extended amygdala-kindling in rats: lack of clear association between development of spontaneous seizures and neuronal damage. Epilepsy Res. 62, 135–156.

Brandt, C., Nozadze, M., Heuchert, N., Rattka, M., Löscher, W., 2010. Disease-modifying effects of phenobarbital and the NKCC1 inhibitor bumetanide in the pilocarpine model of temporal lobe epilepsy. J. Neurosci. 30, 8602–8612.

Brandt, C., Seja, P., Töllner, K., Römermann, K., Hampel, P., Kalesse, M., Kipper, A., Feit, P.W., Lykke, K., Toft-Bertelsen, T.L., Paavilainen, P., Spoljaric, I., Puskarjov, M., Macaulay, N., Kaila, K., Löscher, W., 2018. Bumepamine, a brain-permeant benzylamine derivative of bumetanide, does not inhibit NKCC1 but is more potent to enhance phenobarbital's anti-seizure efficacy. Neuropharmacology 143, 186–204.

Bröer, S., Käufer, C., Haist, V., Li, L., Gerhauser, I., Anjum, M., Bankstahl, M., Baumgärtner, W., Löscher, W., 2016. Brain inflammation, neurodegeneration and seizure development following picornavirus infection markedly differ among virus and mouse strains and substrains. Exp. Neurol. 279, 57–74.

Caceres, M.D., Pfeifer, C.G., Docheva, D., 2018. Understanding Tendons: Lessons from Transgenic Mouse Models. Stem Cells Dev. 27, 1161–1174.

Clayton, J.A., Collins, F.S., 2014. Policy: NIH to balance sex in cell and animal studies. Nature 509, 282–283.

Cleary, R.T., Sun, H., Huynh, T., Manning, S.M., Li, Y., Rotenberg, A., Talos, D.M., Kahle, K.T., Jackson, M., Rakhade, S.N., Berry, G., Jensen, F.E., 2013. Bumetanide enhances phenobarbital efficacy in a rat model of hypoxic neonatal seizures. PLoS One 8, e57148.

Cohen, I., Navarro, V., Clemenceau, S., Baulac, M., Miles, R., 2002. On the origin of interictal activity in human temporal lobe epilepsy in vitro. Science 298, 1418–1421.

Duveau, V., Roucard, C., 2017. A mesiotemporal lobe epilepsy mouse model. Neurochem. Res. 42, 1919–1925.

Duveau, V., Pouyatos, B., Bressand, K., Bouyssieres, C., Chabrol, T., Roche, Y., Depaulis, A., Roucard, C., 2016. Differential effects of antiepileptic drugs on focal seizures in the intrahippocampal kainate mouse model of mesial temporal lobe epilepsy. CNS Neurosci. Ther. 22, 497–506.

Dzhala, V.I., Talos, D.M., Sdrulla, D.A., Brumback, A.C., Mathews, G.C., Benke, T.A., Delpire, E., Jensen, F.E., Staley, K.J., 2005. NKCC1 transporter facilitates seizures in the developing brain. Nat. Med. 11, 1205–1213.

Fisher, R.S., Scharfman, H.E., Decurtis, M., 2014. How can we identify ictal and interictal abnormal activity. Adv. Exp. Med. Biol. 813, 3–23.

Flagella, M., Clarke, L.L., Miller, M.L., Erway, L.C., Giannella, R.A., Andringa, A., Gawenis, L.R., Kramer, J., Duffy, J.J., Doetschman, T., Lorenz, J.N., Yamoah, E.N., Cardell, E.L., Shull, G.E., 1999. Mice lacking the basolateral Na-K-2Cl cotransporter have impaired epithelial chloride secretion and are profoundly deaf. J. Biol. Chem. 274, 26946–26955.

Fritschy, J.M., 2008. Is my antibody-staining specific? How to deal with pitfalls of immunohistochemistry. Eur. J. Neurosci. 28, 2365–2370.

Gröticke, I., Hoffmann, K., Löscher, W., 2008. Behavioral alterations in a mouse model of temporal lobe epilepsy induced by intrahippocampal injection of kainate. Exp. Neurol. 213, 71–83.

Guillemain, I., Kahane, P., Depaulis, A., 2012. Animal models to study aetiopathology of epilepsy: what are the features to model? Epileptic. Disord. 14, 217–225.

Hampel, H., Römermann, K., Gramer, M., Löscher, W., 2021. The search for brain-permeant NKCC1 inhibitors for the treatment of seizures: Pharmacokinetic-pharmacodynamic modelling of NKCC1 inhibition by azosemide, torasemide and bumetanide in mouse brain. Epilepsy Behav. (in press).

Heinrich, C., Lahteinen, S., Suzuki, F., Anne-Marie, L., Huber, S., Haussler, U., Haas, C., Larmet, Y., Castren, E., Depaulis, A., 2011. Increase in BDNF-mediated TrkB signaling promotes epileptogenesis in a mouse model of mesial temporal lobe epilepsy. Neurobiol. Dis. 42, 35–47.

Ho, J., Tumkaya, T., Aryal, S., Choi, H., Claridge-Chang, A., 2019. Moving beyond P values: data analysis with estimation graphics. Nat. Methods 16, 565–566.

Hochman, D.W., 2012. The extracellular space and epileptic activity in the adult brain: explaining the antiepileptic effects of furosemide and bumetanide. Epilepsia 53 (Suppl. 1), 18–25.

Huberfeld, G., Wittner, L., Clemenceau, S., Baulac, M., Kaila, K., Miles, R., Rivera, C., 2007. Perturbed chloride homeostasis and GABAergic signaling in human temporal lobe epilepsy. J. Neurosci. 27, 9866–9873.

Johne, M., Römermann, K., Hampel, P., Gailus, B., Theilmann, W., Ala-Kurikka, T., Kaila, K., Löscher, W., 2021. Phenobarbital and midazolam suppress neonatal seizures in a non-invasive rat model of birth asphyxia while bumetanide is ineffective. Epilepsia in press.

Kahle, K.T., Staley, K.J., 2008. The bumetanide-sensitive Na-K-2Cl cotransporter NKCC1 as a potential target of a novel mechanism-based treatment strategy for neonatal seizures. Neurosurg. Focus. 25, 1–8.

Kahle, K.T., Staley, K.J., Nahed, B.V., Gamba, G., Hebert, S.C., Lifton, R.P., Mount, D.B., 2008. Roles of the cation-chloride cotransporters in neurological disease. Nat. Clin. Pract. Neurol. 4, 490–503.

Kahle, K.T., Simard, J.M., Staley, K.J., Nahed, B.V., Jones, P.S., Sun, D., 2009. Molecular mechanisms of ischemic cerebral edema: role of electroneutral ion transport. Physiology (Bethesda) 24, 257–265.

Kaila, K., Price, T.J., Payne, J.A., Puskarjov, M., Voipio, J., 2014a. Cation-chloride cotransporters in neuronal development. plasticity and disease. Nat. Rev. Neurosci. 15, 637–654.

Kaila, K., Ruusuvuori, E., Seja, P., Voipio, J., Puskarjov, M., 2014b. GABA actions and ionic plasticity in epilepsy. Curr. Opin. Neurobiol. 26, 34–41.

Kang, S.K., Markowitz, G.J., Kim, S.T., Johnston, M.V., Kadam, S.D., 2015. Age- and sex-dependent susceptibility to phenobarbital-resistant neonatal seizures: role of chloride co-transporters. Front. Cell. Neurosci. 9, 173.

Kharod, S.C., Kang, S.K., Kadam, S.D., 2019. Off-Label Use of Bumetanide for Brain Disorders: An Overview. Front. Neurosci. 13, 310.

Kilkenny, C., Browne, W.J., Cuthill, I.C., Emerson, M., Altman, D.G., 2010. Improving bioscience research reporting: the ARRIVE guidelines for reporting animal research. PLoS Biol. 8, e1000412.

Kourdougli, N., Pellegrino, C., Renko, J.M., Khirug, S., Chazal, G., Kukko-Lukjanov, T.K., Lauri, S.E., Gaiarsa, J.L., Zhou, L., Peret, A., Castrén, E., Tuominen, R.K., Crépel, V., Rivera, C., 2017. Depolarizing g-aminobutyric acid contributes to glutamatergic network rewiring in epilepsy. Ann. Neurol. 81, 251–265.

Koyama, R., Tao, K., Sasaki, T., Ichikawa, J., Miyamoto, D., Muramatsu, R., Matsuki, N., Ikegaya, Y., 2012. GABAergic excitation after febrile seizures induces ectopic granule cells and adult epilepsy. Nat. Med. 18, 1271–1278.

Lassmann, H., Petsche, U., Kitz, K., Baran, H., Sperk, G., Seitelberger, F., Hornykiewicz, O., 1984. The role of brain edema in epileptic brain damage induced by systemic kainic acid injection. Neuroscience 13, 691–704.

Li, X., Zhou, J., Chen, Z., Chen, S., Zhu, F., Zhou, L., 2008. Long-term expressional changes of Na+ -K+ -Cl- co-transporter 1 (NKCC1) and K+ -Cl- co-transporter 2 (KCC2) in CA1 region of hippocampus following lithium-pilocarpine induced status epilepticus PISE. Brain Res. 1221, 141–146.

Liu, R., Wang, J., Liang, S., Zhang, G., Yang, X., 2020. Role of NKCC1 and KCC2 in Epilepsy: From Expression to Function. Front. Neurol. 10, 1407.

Löscher, W., Puskarjov, M., Kaila, K., 2013. Cation-chloride cotransporters NKCC1 and KCC2 as potential targets for novel antiepileptic and antiepileptogenic treatments. Neuropharmacology 69, 62–74.

Lydersen, S., Fagerland, M.W., Laake, P., 2009. Recommended tests for association in 2 x 2 tables. Stat. Med 28, 1159–1175.

Marguet, S.L., Le Schulte, V.T., Merseburg, A., Neu, A., Eichler, R., Jakovcevski, I., Ivanov, A., Hanganu-Opatz, I.L., Bernard, C., Morellini, F., Isbrandt, D., 2015. Treatment during a vulnerable developmental period rescues a genetic epilepsy. Nat. Med 21, 1436–1444.

Markadieu, N., Delpire, E., 2014. Physiology and pathophysiology of SLC12A1/2 transporters. Pflugers Arch. 466, 91–105.

Maroso, M., Balosso, S., Ravizza, T., Iori, V., Wright, C.I., French, J., Vezzani, A., 2011. Interleukin-1beta biosynthesis inhibition reduces acute seizures and drug resistant chronic epileptic activity in mice. Neurotherapeutics. 8, 304–315.

McCloskey, D.P., Hintz, T.M., Pierce, J.P., Scharfman, H.E., 2006. Stereological methods reveal the robust size and stability of ectopic hilar granule cells after pilocarpine-induced status epilepticus in the adult rat. Eur. J. Neurosci. 24, 2203–2210.

Miles, R., Blaesse, P., Huberfeld, G., Wittner, L., Kaila, K., 2012. Chloride homeostasis and GABA signaling in temporal lobe epilepsy. In: Noebels, J.L., Avoli, M., Rogawski, M.A., Olsen, R.W., Delgado-Escueta, A.V. (Eds.), Jasper's Basic Mechanisms Of The Epilepsies, Fourth edition. Oxford University Press, New York, pp. 581–590.

Mokgokong, R., Wang, S., Taylor, C.J., Barrand, M.A., Hladky, S.B., 2014. Ion transporters in brain endothelial cells that contribute to formation of brain interstitial fluid. Pflugers Arch. 466, 887–901.

Müller, C.J., Gröticke, I., Hoffmann, K., Schughart, K., Löscher, W., 2009. Differences in sensitivity to the convulsant pilocarpine in substrains and sublines of C57BL/6 mice. Genes Brain Behav. 8, 481–492.

Munoz, A., Mendez, P., DeFelipe, J., Alvarez-Leefmans, F.J., 2007. Cation-chloride cotransporters and GABA-ergic innervation in the human epileptic hippocampus. Epilepsia 48, 663–673.

Nardou, R., Ben Ari, Y., Khalilov, I., 2009. Bumetanide, an NKCC1 antagonist, does not prevent formation of epileptogenic focus but blocks epileptic focus seizures in immature rat hippocampus. J. Neurophysiol. 101, 2878–2888.

Ndode-Ekane, X.E., Pitkänen, A., 2013. Urokinase-type plasminogen activator receptor modulates epileptogenesis in mouse model of temporal lobe epilepsy. Mol. Neurobiol. 47, 914–937.

Okabe, A., Yokokura, M., Toyoda, H., Shimizu-Okabe, C., Ohno, K., Sato, K., Fukuda, A., 2003. Changes in chloride homeostasis-regulating gene expressions in the rat hippocampus following amygdala kindling. Brain Res. 990, 221–226.

Pathak, H.R., Weissinger, F., Terunuma, M., Carlson, G.C., Hsu, F.C., Moss, S.J., Coulter, D.A., 2007. Disrupted dentate granule cell chloride regulation enhances synaptic excitability during development of temporal lobe epilepsy. J. Neurosci. 27, 14012–14022.

Paxinos, G., Franklin, K.B.J., 2012. In: Paxinos, G., Franklin, K.B.J. (Eds.), The Mouse Brain in Stereotaxic Coordinates, 4th edition. Academic Press, New York.

Puskarjov, M., Kahle, K.T., Ruusuvuori, E., Kaila, K., 2014. Pharmacotherapeutic targeting of cation-chloride cotransporters in neonatal seizures. Epilepsia 55, 806–818.

Riban, V., Bouilleret, V., Pham, L., Fritschy, J.M., Marescaux, C., Depaulis, A., 2002. Evolution of hippocampal epileptic activity during the development of hippocampal sclerosis in a mouse model of temporal lobe epilepsy. Neuroscience 112, 101–111.

Rivera, C., Li, H., Thomas-Crusells, J., Lahtinen, H., Viitanen, T., Nanobashvili, A., Kokaia, Z., Airaksinen, M.S., Voipio, J., Kaila, K., Saarma, M., 2002. BDNF-induced TrkB activation down-regulates the K+-Cl- cotransporter KCC2 and impairs neuronal Cl- extrusion. J. Cell Biol. 159, 747–752.

Russell, J.M., 2000. Sodium-potassium-chloride cotransport. Physiol. Rev. 80, 211–276.

Sandau, U.S., Yahya, M., Bigej, R., Friedman, J.L., Saleumvong, B., Boison, D., 2019. Transient use of a systemic adenosine kinase inhibitor attenuates epilepsy development in mice. Epilepsia 60, 615–625.

Scharfman, H.E., Pierce, J.P., 2012. New insights into the role of hilar ectopic granule cells in the dentate gyrus based on quantitative anatomic analysis and three-dimensional reconstruction. Epilepsia 53 (Suppl. 1), 109–115.

Schidlitzki, A., Twele, F., Klee, R., Waltl, I., Römermann, K., Broer, S., Meller, S., Gerhauser, I., Rankovic, V., Li, D., Brandt, C., Bankstahl, M., Töllner, K., Löscher, W., 2017. A combination of NMDA and AMPA receptor antagonists retards granule cell dispersion and epileptogenesis in a model of acquired epilepsy. Sci. Rep. 7, 12191.

Schidlitzki, A., Bascunana, P., Srivastava, P.K., Welzel, L., Twele, F., Töllner, K., Käufer, C., Gericke, B., Feleke, R., Meier, M., Polyak, A., Ross, T.L., Gerhauser, I., Bankstahl, J.P., Johnson, M.R., Bankstahl, M., Löscher, W., 2020. Proof-of-concept that network pharmacology is effective to modify development of acquired temporal lobe epilepsy. Neurobiol. Dis. 134, 104664.

Schmittgen, T.D., Livak, K.J., 2008. Analyzing real-time PCR data by the comparative C (T) method. Nat. Protoc. 3, 1101–1108.

Simard, J.M., Kahle, K.T., Gerzanich, V., 2010. Molecular mechanisms of microvascular failure in central nervous system injury–synergistic roles of NKCC1 and SUR1/TRPM4. J Neurosurg. 113, 622–629.

Sipilä, S.T., Huttu, K., Yamada, J., Afzalov, R., Voipio, J., Blaesse, P., Kaila, K., 2009. Compensatory enhancement of intrinsic spiking upon NKCC1 disruption in neonatal hippocampus. J. Neurosci. 29, 6982–6988.

Sivakumaran, S., Maguire, J., 2016. Bumetanide reduces seizure progression and the development of pharmacoresistant status epilepticus. Epilepsia 57, 222–232.

Stamboulian-Platel, S., Legendre, A., Chabrol, T., Platel, J.C., Pernot, F., Duveau, V., Roucard, C., Baudry, M., Depaulis, A., 2016. Activation of GABA(A) receptors controls mesiotemporal lobe epilepsy despite changes in chloride transporters expression: In vivo and in silico approach. Exp. Neurol. 284, 11–28.

Suzuki, F., Junier, M.P., Guilhem, D., Sorensen, J.C., Onteniente, B., 1995. Morphogenetic effect of kainate on adult hippocampal neurons associated with a prolonged expression of brain-derived neurotrophic factor. Neuroscience 64, 665–674.

Töllner, K., Brandt, C., Töpfer, M., Brunhofer, G., Erker, T., Gabriel, M., Feit, P.W., Lindfors, J., Kaila, K., Löscher, W., 2014. A novel prodrug-based strategy to increase effects of bumetanide in epilepsy. Ann. Neurol. 75, 550–562.

Twele, F., Töllner, K., Brandt, C., Löscher, W., 2016a. Significant effects of sex, strain, and anesthesia in the intrahippocampal kainate mouse model of mesial temporal lobe epilepsy. Epilepsy Behav. 55, 47–56.

Twele, F., Töllner, K., Bankstahl, M., Löscher, W., 2016b. The effects of carbamazepine in the intrahippocampal kainate model of temporal lobe epilepsy depend on seizure definition and mouse strain. Epilepsia Open 1, 45–60.

Vanhatalo, S., Hellstrom-Westas, L., De Vries, L.S., 2009. Bumetanide for neonatal seizures: Based on evidence or enthusiasm? Epilepsia 50, 1292–1293.

Virtanen, M.A., Uvarov, P., Hübner, C.A., Kaila, K., 2020. NKCC1, an Elusive Molecular Target in Brain Development: Making Sense of the Existing Data. Cells 9, 2607.

Wallace, B.K., Foroutan, S., O'Donnell, M.E., 2011. Ischemia-induced stimulation of Na-K-Cl cotransport in cerebral microvascular endothelial cells involves AMP kinase. Am. J. Physiol Cell Physiol 301, C316–C326.

Wilson, C.S., Mongin, A.A., 2019. The signaling role for chloride in the bidirectional communication between neurons and astrocytes. Neurosci. Lett. 689, 33–44.

Zhu, L., Polley, N., Mathews, G.C., Delpire, E., 2008. NKCC1 and KCC2 prevent hyperexcitability in the mouse hippocampus. Epilepsy Res. 79, 201–212.